AD613485

A STUDY OF

JET EJECTOR PHENOMENA

By

Chia-An Wan

Research Report No. 57   November 1964

AEROPHYSICS

MISSISSIPPI STATE UNIVERSITY

A STUDY OF

JET EJECTOR PHENOMENA

By

Chia-An Wan

Research Report No. 57   November 1964

Conducted For

OFFICE OF NAVAL RESEARCH

Under

CONTRACT NONR 978(03)

By

The Aerophysics Department

Mississippi State University

CONTENTS

ILLUSTRATIONS

iv

TABLES

SYMBOLS

A	Cross section area of exit of nozzle, in^2
A_e	Cross section area of ejector, in^2
D	Diameter of exit of nozzle, in
D_e	Diameter of ejector, in
k	Slope of $\frac{U_e}{U}$ vs l/D curve
l	Length of gap, in
L	Length of ejector, in
m	Inverse of exponent related to velocity profile at outlet of ejector, defined in Equation 2
n	Exponent related to velocity profile, defined in Equation 36
p	Local pressure, lb/in^2
p_a	Pressure of the atmosphere, lb/in^2
p_o	Pressure at exit of nozzle, lb/in^2
p_1	Pressure at initial plane, lb/in^2
p_2	Pressure at outlet of ejector, lb/in^2
$\bar{R}$	Reynolds Number, $\frac{Re\,U_1}{2\nu}$
R	Radius of exit of nozzle, in
Re	Radius of ejector, in
r	Distance measured in radial direction from ejector centerline, in
r_c	Radius of the laminar core, in
T	Thrust force of jet ejector with no gap, lb
Tg	Thrust force of jet ejector with gap, lb

T_j	Thrust force on jet flow, lb
u	Axial velocity, ft/sec
U	Centerline axial velocity, ft/sec
U_o	Axial velocity at the exit of nozzle, ft/sec
U_1	Secondar_ or induced flow velocity at initial plane, ft/sec
u_2, U_2	Velocity at the outlet of ejector and its centerline value, ft/sec
U_p	Potential velocity beyond the edge of the jet, ft/sec
v	Radial velocity, ft/sec
w	Distance in radial direction from edge of the laminar core, in
W	Distance in radial direction from the edge of the laminar core to the edge of jet, in
x	Axial distance from the initial plane, in
x_k	Length of the laminar core, in
x_m	Length of the modified free mixing flow regime, in
y	Distance in the radial direction from the centerline of the ejector to the edge of the jet, in
y_k	Radius of the jet at $x = x_k$, in
z	Distance in the radial direction from the walls of the ejector, in
α_1	Induced velocity ratio at initial plane, $\dfrac{U_1}{U_o}$
α_2	Velocity ratio at outlet of ejector, $\dfrac{U_2}{U_o}$
μ	Area ratio, $\dfrac{A_e}{A}$
φ	Augmentation factor without gap, $\dfrac{T}{T_j}$
φ_G	Augmentation factor with gap, $\dfrac{T_G}{T}$
φ_T	Overall augmentation factor, $\dfrac{T_G}{T_j}$
ρ	Density of air, $\dfrac{lb\,sec^2}{ft^4}$

τ Shear stress, lb/in^2

δ Thickness of boundary layer of the walls of ejector, in

ν Kinetic viscosity of air, ft^2/sec

INTRODUCTION

A jet ejectro, or jet pump as it is sometimes called, is a device in which a fluid is emitted from an orifice or nozzle exit into a hollow, generally cylindrical, body. Due to the shear stresses between the moving fluid and the ambient still fluid, part of the kinetic energy of the moving is transferred to the still fluid. In the case of a constant-pressure mixing tube, which can be made through careful design, (Reference 1), this mixing process is the primary cause of secondary or induced flow.

However, in the case of a constant-area mixing tube, a low-pressure field is created by the jet flow. This difference in pressure between the exit plane of the nozzle and the ambient fluid upstream causes an entrainment of the ambient fluid or a secondary flow. Due to the transfer of energy, the secondary flow is either accelerated or pumped to a higher pressure. The jet flow and its induced flow are not necessarily of the same fluid; either of them can be air, water, steam, or the exhausted gas of a jet engine. The ejector is not necessarily circular, but can be of any shape, as required by the physical installation.

The principle of a confined jet flow finds many different applications in industry, especially the aerospace industry. An ejector can be used as a pump, blower-augmenter, and noise-reducer. (References 2, 3, 4, 5, 6, 7, 8, 9, 10, 11, 12). In case the jet ejector is operated with no change in pressure it does not provide a pumping effect. However, it does provide a thrust increase for the installation.

A typical constant-area jet ejector arrangement is shown schematically in Figure 1. With this arrangement, the primary jet flow is emitted from the exit of the nozzle into the ejector, and the velocity is almost uniformly distributed throughout the cross section area of the exit of the nozzle. A subatmospheric pressure field is created, which consequently causes a secondary flow in the rest of the cross section area of the ejector at the initial plane. If the boundary layer growth along the contour of the faired inlet of the ejector is neglected, the secondary velocity distribution can be considered to be constant.

The velocity of the secondary flow is less than that of the primary flow. As a consequence, there is a near discontinuity in the velocity profile across the ejector in the initial plane. Downstream of this plane, a process of turbulent mixing tends to smooth out this near discontinuity so that, if the ejector is long enough, the mixed flow velocity profile becomes that of fully developed turbulent pipe flow.

Since the static pressure increases downstream of the initial plane until, at the outlet of the ejector, it becomes equal to that of the

1

surrounding atmosphere, the static pressure increase per unit length of
the ejector depends upon the total length of the ejector. The mass rate
flow remains constant throughout the length of the ejector, but total
momentum at the outlet of the ejector is less than that at the initial
plane due to losses which result from skin friction.

The maximum augmentation factor for a straight ejector is 2.0 as
calculated theoretically by von Karman. (Reference 6). He assumed that
the velocity distributed was uniform at the outlet of the ejector, and
that skin friction losses were negligible. A similar calculation has
been performed in this report using somewhat different assumptions.

A knowledge of the free-mixing process and pipe flows aids in
understanding the confined-mixing process. Information concerning those
phenomena can be found in many works. (References 13, 14, 15, 16, 17,
18, 19, 20, 21). The equations of motion for the flow field of a
constant-pressure mixing tube is similar to that of a free jet flow,
however, the boundary conditions are different. The axial pressure
gradient term in the equation of motion for a constant-area mixing tube
and the coexistence of laminar and turbulent flows make the flow field
difficult for mathematical analysis.

For comparison purposes a satisfactory solution of the problem of
a constant-area mixing process can be obtained by approximate solution
of the Naview-Stokes equations. However, this approach requires such a
great amount of work that it becomes questionable whether the approxi-
mate solution justifies the effort. As a consequence, this report adopts
an approach in which the author uses existing theories and empirical
formulae to solve the problem.

EXPERIMENTAL APPARATUS AND TECHNIQUES

For the sake of convenience, two sets of experimental apparatus were used - one for measuring the thrust forces and one for measuring the velocity distributions. Two convergent nozzles and three constant-area ejectors were used in both measurements; with one constant-area ejector of relatively long length being used in velocity distribution measurements only. Compressed air used in both measurements was supplied by the equipment shown schematically in Figure 2. Thrust forces were measured with the device shown in Figure 3a.

In order to change the relative location of the exit of the nozzle, brass tubes were used as extensions of the nozzle exit. (Figure 4). Their dimensions are shown in Table 1.

Ejectors of various lengths were attached to the primary nozzle as shown in Figure 3b. Care was taken to insure that the ejector and primary nozzle were aligned axially. The dimensions of the ejectors are shown in Table 2.

By using these nozzles and ejectors, the area ratio of the jet ejector could be varied from 4.0 to 105.5.

The primary nozzle flow and the secondary entrained flow could be calculated from velocity profiles measured at various locations in the ejector by means of a pitot-static tube. This tube was attached to a micrometer-type mechanism which allowed it to be positioned at any desired location along the diameter of the ejector. (Figure 5). Velocities were measured by means of a U-tube water manometer.

Profiles were measured at the distances downstream of the initial plane as shown in Table 3.

All velocity profiles and static pressure were measured when the nozzle and ejector were positioned horizontally. (Figure 6). All thrust force measurements were made with the apparatus positioned vertically.

Thrust forces of the nozzles were first measured at various gauge pressures as shown in Figure 7. These measurements were then repeated with the ejector attached and were plotted against gauge pressure. Typical curves are shown in Figure 8. At an arbitrary gauge pressure of 35 p.s.i. the augmentation factor was obtained by dividing the thrust of the jet with ejector by the thrust of the jet without ejector. The effect of the length ratio on augmentation factor is shown in Figure 9.

3

The thrust forces of the jet ejectors at different gaps were measured. These forces were divided by the thrust of the jet ejectors with no gap in order to obtain the gap augmentation factor φ_G, and were similarily divided by the thrust of the jet in order to obtain the overall augmentation factor, φ_T. φ_G and φ_T are plotted against gap ratio in Figure 10. Gap is the distance between the nozzle exit plane and the initial plane of the ejector. The initial plane is defined as the plane of the ejector where the faired inlet of the ejector ends and the constant-area portion of the ejector begins. Gap is defined as negative when the exit of the nozzle is inserted into the ejector, as positive when the exit is away from the ejector, and as zero when the nozzle exit plane coincides with the initial plane of the ejector.

THEORETICAL CONSIDERATIONS

Several assumptions are made in the theoretical considerations. They are:

1. The flow is incompressible, hence the static pressure is constant throughout the initial plane within the ejector and the pressure at the outlet of the ejector is equal to that of the surrounding atmosphere.

2. The velocity at the exit of the nozzle is uniformly distributed, i.e., the velocity profile is constant.

3. The secondary flow velocity is uniformly distributed at the initial plane

4. There is no pressure change in the radial direction.

5. The flow field is of an axisymmetric case.

A. Thrust Augmentation Factor and Velocity Ratios

A method similar to that used by von Karman (Reference 6) was used in calculating the thrust augmentation factor and the velocity ratios. It was also assumed that

1. The velocity distribution at the exit of the ejector follows the relation:
$$\frac{U_2}{U_2} = \left(\frac{Z}{Re}\right)^{\frac{1}{m}}$$

2. Skin friction losses are negligible.

3. The walls of the nozzle are infinitely thin at the initial plane.

4. The velocities at the nozzle exit remain unchanged by the installation of the ejector.

The equation of continuity may be written as:

$$\rho A U_0 + \rho (Ae - A) U_1 = \rho \int_0^{Re} 2\pi U_2 Z dZ$$

5

After dividing throughout by $\rho A U_e$, one may write the equation as

$$1 + (\mu - 1)\alpha_1 = 2\mu\alpha_2 \int_0^1 \left(\frac{U_2}{U_2}\right)\left(\frac{z}{Re}\right) d\left(\frac{z}{Re}\right).$$

(1)

Using the assumption that

$$\left(\frac{U_2}{U_2}\right) = \left(\frac{z}{Re}\right)^{\frac{1}{m}},$$

(2)

equation 1 may be rewritten as

$$1 + (\mu - 1)\alpha_1 = \frac{2m}{2m+1} \mu\alpha_2.$$

(3)

The momentum equation may be written as

$$A(\rho U_o^2 + p_o) + (A_e - A)(\rho U_1^2 + p_1) = \int_0^{Re}(\rho U_2^2 + p_2) 2\pi z \, dz,$$

where $p_1 = p_o$, $p_2 = p_a$ and according to Bernoulli's theory

$$p_a = p_1 + \frac{1}{2}\rho U_1^2$$

(4)

The momentum equation may be rewritten as

$$1 + \frac{1}{2}\alpha_1^2 (\mu - 2) = 2\alpha_2^2 \mu \int_0^1 \left(\frac{U_2}{U_2}\right)^2 \left(\frac{z}{Re}\right) d\left(\frac{z}{Re}\right).$$

Integrating the term on the right-hand side results in

$$1 + \frac{1}{2}\alpha_1^2 (\mu - 2) = \frac{m}{m+1} \mu\alpha_2^2.$$

(5)

Solving the velocity ratios from equations 3 and 5 for $m = 4$,

$$\alpha_1 = \frac{-\left[\frac{81}{40}\frac{\mu-1}{\mu}\right] + \sqrt{\left(\frac{81}{40}\frac{\mu-1}{\mu}\right)^2 - 4\left[\frac{81}{80}\frac{(\mu-1)^2}{\mu} - \frac{1}{2}(\mu-2)\right]\left[\frac{81}{80\mu} - 1\right]}}{2\left[\frac{81}{80}\frac{(\mu-1)^2}{\mu} - \frac{1}{2}(\mu-2)\right]}$$

(6)

and

$$\alpha_2 = \frac{9}{8\mu}\left\{1 + (\mu-1)\frac{\sqrt{\left(\frac{81}{40}\frac{\mu-1}{\mu}\right)^2 - 4\left[\frac{81}{80}\frac{(\mu-1)^2}{\mu} - \frac{1}{2}(\mu-2)\right]\left[\frac{81}{80\mu} - 1\right]} - \frac{81}{40}\frac{\mu-1}{\mu}}{2\left[\frac{81}{80}\frac{(\mu-1)^2}{\mu} - \frac{1}{2}(\mu-2)\right]}\right.$$

(7)

6

If μ is much greater than 1.0, equations 6 and 7 may be simplified and rewritten as

$$\alpha_1 = \frac{\sqrt{\left(\frac{81}{40}\right)^2 - 4\left[\frac{41}{80}\mu - \frac{1}{80}\right]\left[\frac{81}{80}\frac{1}{\mu} - 1\right]} - \frac{81}{40}}{2\left[\frac{41}{80}\mu - \frac{1}{80}\right]}$$

(8)

$$\text{and } \alpha_2 = \frac{9}{8\mu}\left[1 + (\mu-1)\frac{\sqrt{\left(\frac{81}{40}\right)^2 - 4\left[\frac{41}{80}\mu - \frac{1}{80}\right]\left[\frac{81}{80}\frac{1}{\mu} - 1\right]} - \frac{81}{40}}{2\left[\frac{41}{80}\mu - \frac{1}{80}\right]}\right].$$

(9)

The thrust augmentation factor, φ, is defined by the formula

$$\varphi = \frac{\int_0^{Re} \rho u_2^2 z\, dz}{\rho A U_0^2}$$

Carrying out the calculation, one has for the thrust augmentation factor,

$$\varphi = \frac{4}{5}\mu\,(\alpha_2)^2.$$

(10)

It is somewhat arbitrary to define the thrust augmentation factor as the ratio of the actual thrust to the product of the mass and the velocity of the jet instead of to its total impulse. However, in general, the difference is not large.

In Figure 12 the thrust augmentation factor, φ, is shown. Velocity ratios α_1 and α_2 are plotted in Figure 13, showing comparison with the experimental measurements.

The pressure reduction may be obtained by using equation 4

$$\frac{p_a - p_1}{\frac{1}{2}\rho U_0^2} = (\alpha_1)^2 = \left[\frac{\sqrt{\left(\frac{81}{40}\right)^2 - 4\left(\frac{41}{80}\mu - \frac{1}{80}\right)\left(\frac{81}{80}\frac{1}{\mu} - 1\right)} - \frac{81}{40}}{2\left[\frac{41}{80}\mu - \frac{1}{80}\right]}\right]^2$$

This equation has been plotted in Figure 14.

B. **Structure of the Flow Field in the Inlet Length of the Ejector**

The structure of the flow field at the inlet of the ejector is very complicated (Figure 1). As the compressed air is emitted from the nozzle

7

into the constant-area ejector, there is a field of subatmospheric
pressure created. Consequently, a secondary flow of constant velocity
is formed at the inlet of the ejector. Disregarding the faired portion of
the inlet, the boundary layers at the wall are infinitely thin at the
initial plane. Normal boundary layer growth occurs downstream from the
initial plane. Disregarding the flow of the jet, the boundary layers
keep growing, until they meet at a point on the axis of the pipe. Until
this happens, there is a core of fluid practically uninfluenced by
viscous effects in which the total head may be considered constant.
This problem of inlet flow of a circular pipe had been investigated by
Goldstein (Reference 22), Langhaar (Reference 23), Schiller (Reference
24), and Talbot (Reference 25).

Due to the existence of the jet flow, the edge of the wall boundary
layers will not meet at a point on the axis of the pipe; instead they
join the boundary of the jet.

The flow field in the inlet portion of the ejector, disregarding
the primary jet flow, becomes similar to the case studied by Schiller.
Schiller suggested that the wall boundary layer thickness, δ, is
related to the velocities, U_1 and U_p, by the following relationship,

$$\delta = 2\,Re - Re\sqrt{6\left(\frac{U_1 - U_P}{U_P}\right) + 4}\,,$$
(11)

where Re is the radius of the circular tube, U_1 is the constant velocity
of the potential core at the initial plane and U_p is the velocity in the
potential core which is a function of x.

The velocities have been related to the axial coordinate as

$$\frac{x}{Re} = \frac{1}{4}\,\overline{R}\,f(\eta),$$
(12)

where $\overline{R} = \dfrac{Re\,U_1}{\nu}$ is the Reynolds Number, and

$$\eta = \frac{U_P}{U_1} - 1.$$
(13)

The function $f(\eta)$ has been given by Schiller as

$$f(\eta) = \left[\frac{58}{15}\eta - \frac{66}{15}\ln(1+\eta) - \frac{17}{15}\sqrt{4 + 2\eta - 2\eta^2}\right.$$
$$-\frac{48}{15}\sqrt{2}\sqrt{\frac{2-\eta}{1+\eta}} + \frac{130}{15} - \frac{63}{15}\sqrt{2}\,\sin^{-1}\sqrt{\frac{1}{3} + \frac{\eta}{3}}$$
$$+\frac{63}{15}\sqrt{2}\,\sin^{-1}\sqrt{\frac{1}{3}} - \frac{48}{15\sqrt{2}}\sin^{-1}\left(\frac{2}{3}\eta - \frac{1}{3}\right) - \frac{48}{15\sqrt{2}}\left.\sin^{-1}\frac{1}{3}\right],$$
(14)

and has been simplified by Goldstein to the following form which has
been plotted in Figure 11,

$$f(\eta) = \frac{1}{8}\left[\frac{58}{15}\eta - \frac{22}{5}\ln(1+\eta) - \frac{17}{15}\sqrt{4+2\eta-2\eta^2}\right.$$
$$\left. -\frac{16}{5}\left(\frac{4-2\eta}{1+\eta}\right)^{\frac{1}{2}} - \frac{37\sqrt{2}}{10}\sin^{-1}\frac{2\eta-1}{3} + \frac{26}{3} - \frac{37}{10\sqrt{2}}\sin^{-1}\frac{1}{3}\right]. \tag{15}$$

For the sake of simplicity, one can approximate the curve of
equation 15 by

$$f(\eta) = 0.00133\eta + 0.05625\eta^2 + 0.00208\eta^3. \tag{16}$$

Equation 16 is plotted in Figure 11 for comparison with equation 15.

Since the thickness of the wall boundary layer, δ, is an explicit
function of U_p (equation 11), U_p is an implicit function of x
(equation 12). Consequently, δ is a function of x also. δ/Re is
plotted against the nondimensional variable $\frac{4}{R}\left(\frac{x}{Re}\right)$ in Figure 15.

The variation of the radius of the mixing zone can be estimated by
a straight line. Starting with the equation given by Helmbold (Refer-
ence 26), for a mixing tube of constant pressure,

$$\frac{y_k}{R} = 1.723 + 0.467(1-\alpha_1) + 0.25(1-\alpha_1)^2, \tag{17}$$

where y_k denotes the radius of the mixing zone at the end of the laminar
core of the jet flow. Hence,

$$\frac{y-R}{x} = \frac{y_k-R}{x_k},$$

where x_k, as given by Helmbold, expressing the length of the laminar
core, is

$$\frac{x_k}{R} = \frac{11.6}{1-\alpha_1} - 2.5(1-\alpha_1). \tag{18}$$

Thus,

$$\frac{y}{R} = \frac{\frac{x}{R}}{\frac{11.6}{1-\alpha_1} - 2.5(1-\alpha_1)}\left[1.723 + 0.467(1-\alpha_1) + 0.25(1-\alpha_1)^2 - 1\right] + 1. \tag{19}$$

By equating the radius of the mixing zone $(Re - \delta)$, one can find
the location where the wall boundary layer joins the boundary of the
mixing zone.

9

The primary flow, except in the turbulent boundary layer at the wall of the nozzle, emerges as a laminar jet with uniform velocity which, beginning at the rim of the nozzle, becomes increasingly turbulent downstream as the mixing of primary and secondary flow spreads inward. The length of the laminar core has been investigated by many authors. For a free jet, according to Faris (Reference 15), it is 4.3 nozzle diameters, which compares favorably with Keuthe's 4.44 nozzle diameters (Reference 14), and Davies' 4.35 nozzle diameters (Reference 17); but for confined jet flow, it depends on area ratio.

For the confined jet flow of the present case, the dimensions of the core could be computed by the following formulae derived from the results of Szablesaki's calculation by Helmbold (Reference 26), valid for the case of a confined jet with constant pressure across the ejector. The length of the laminar core in terms of nozzle radius is

$$\frac{X_k}{R} = \frac{11.6}{1-\alpha_1} - 2.5(1-\alpha_1).$$

(18)

The radius of the mixing zone at the distance $x = x_k$ is

$$\frac{Y_k}{R} = 1.723 + 0.467(1-\alpha_1) + 0.25(1-\alpha_1)^2.$$

A comparison of the lengths of the laminar core is presented in Figure 16.

C. Velocity Distribution Near the Inlet of the Ejector

The velocity distribution of a confined jet flow has been investigated by many authors, such as Cruse and Tontini (Reference 1), Helmbold (References 26, 27, 28) and Squire and Trouncer (Reference 29).

Since the flow is almost parallel and the pressure is constant over any cross section area of the ejector, the simplified form of the boundary layer equations is justified here. The equation of motion is

$$u\frac{\partial u}{\partial x} + v\frac{\partial u}{\partial r} = -\frac{1}{\rho}\frac{dp}{dx} + \frac{1}{\rho r}\frac{\partial(r\tau)}{\partial r}.$$

(21)

Following the apparent viscosity theory of Prandtl (Reference 21), the shearing stress, τ, may be expressed as $\tau = \rho\epsilon\frac{\partial u}{\partial r}$,

(22)

10

where ϵ , the so called virtual kinematic viscosity, could be written as

$$\epsilon = \mathcal{H} y (\bar{u}_{max} - \bar{u}_{min}).$$

(23)

$\mathcal{H}$ is a constant, and Y is the radius of the boundary of the jet before the boundary meets the edges of the boundary layers of the walls of the ejector. $\bar{u}_{max}$, in the present report, is the centerline velocity U and $\bar{u}_{min}$ is the potential velocity U_p outside the boundary of the spreading of the jet.

Thus, the shearing stress, following the terminology used in this report, could be written as

$$\tau = \rho \mathcal{H} y(x)(U - U_p)(\frac{\partial u}{\partial r}).$$

(24)

Substituting the expression for the shearing stress into the original equation of motion (equation 21), one has

$$u \frac{\partial u}{\partial x} + v \frac{\partial u}{\partial r} = -\frac{1}{\rho} \frac{dp}{dx} + \mathcal{H} y(x)(1 - u_p)\frac{1}{r}\frac{\partial}{\partial r}\left[r(\frac{\partial u}{\partial r})\right]$$

(25)

It seems reasonable to assume the radial velocity component, v, disappears at the outer potential flow zone. Since the axial velocity component is a function of x only, the equation of motion, within the potential flow zone, can be simplified to

$$\frac{dp}{dx} + \rho U_p \frac{dU_p}{dx} = 0.$$

(26)

Consequently, the equation of motion can be rewritten as

$$u \frac{\partial u}{\partial x} + v \frac{\partial u}{\partial r} = U_p \frac{dU_p}{dx} + \mathcal{H}(y(x)(U - U_p)\frac{1}{r}\frac{\partial}{\partial r}\left[r(\frac{\partial u}{\partial r})\right].$$

(27)

As suggested by Helmbold, the axial velocity component, u, may be written as

$$u = \bar{U}_p(x) + \Delta U(x) f(x, r),$$

(28)

where $\Delta U(x) = U(x) - U_p(x).$

11

Substituting equation 28 into equation 27, one has

$$(U_p + \Delta U f)(U_p' + \Delta U' f + \Delta U f_x') + v \Delta U f_r' = U_p U_p' + \varkappa y \Delta U^2 (\tfrac{f_r'}{r} + f_{rr}''),$$ (29)

where

$$U_p' = \frac{dU_p}{dx}, \quad \Delta U' = \frac{d \Delta U}{dx}, \quad f_r' = \frac{\partial f}{\partial r}, \quad f_x' = \frac{\partial f}{\partial x},$$

and

$$f_{rr}'' = \frac{\partial^2 f}{\partial r^2}.$$

If the law of similarity holds,

$$f = f\left[\frac{r}{y(x)}\right]; \quad f_r' = \frac{1}{y(x)} \frac{df}{d\left[\frac{r}{y(x)}\right]},$$

and

$$f_x' = -\frac{r}{y(x)} \frac{d y(x)}{dx} f_r'.$$

The boundary conditions are as follows:

at $r = 0$: $\quad f = 1, \quad$ hence $\quad f_x' = 0$
$\qquad\qquad f_r' = 0$
$\qquad\qquad v = 0$ (30)

at $r = y(x)$:

$\qquad\qquad f = 0 \quad f_r' = 0$
$\quad$ hence $f_x' = 0$ (31)

As a consequence,

at $r = 0$,

$$(U_p + \Delta U)(U_p' + \Delta U') = U_p U_p' + \varkappa y(x) \Delta U^2 \lim_{r \to 0} (\tfrac{f_r'}{r} + f_{rr}'')$$

or

$$\varkappa y(x) \lim_{r \to 0} (\tfrac{f_r'}{r} + f_{rr}'') = (1 + \tfrac{U_p}{\Delta U}) \tfrac{\Delta U'}{\Delta U} + \tfrac{U_p'}{\Delta U}.$$ (32)

12

At $r = y(x)$,

$$U_p U_p' = U_p U_p' + \varkappa y(x) \Delta U^2 f \dot{r} \dot{r},$$

or

$$f \ddot{r} (y) = 0. \tag{33}$$

Helmbold had, for the sake of simplicity, suggested the function

$$f = \left[1 - \left(\frac{r}{y} \right)^2 \right]^4. \tag{34}$$

This function satisfies the boundary conditions of equation 33 and of equations 30 and 31.

Faris (Reference 15), in studying the free jet mixing, used the velocity distribution suggested by Cornish (Reference 13):

$$\frac{u}{U} = \frac{1}{2} \left[1 - \cos \pi \left\{ 1 - \left(1 - (0.5)^{\frac{1}{n}} \right) \frac{w}{w_{\frac{1}{2}}} \right\}^n \right], \tag{35}$$

where n is an empirical function of the axial coordinate, x varies between 1.0 and 2.0, and $w_{\frac{1}{2}}$ denotes the w where $\frac{u}{U} = \frac{1}{2}$.

Equation 35 should be changed so that it can be relevant and compared with the measurements of the present investigation. Equation 35 becomes

$$\frac{u - U_p}{U - U_p} = \frac{1}{2} \left[1 - \cos \pi \left\{ 1 - \left[1 - (0.5)^{\frac{1}{n}} \right] \frac{w}{w_{\frac{1}{2}}} \right\}^n \right], \tag{36}$$

where $w_{\frac{1}{2}}$ denotes the w where $\frac{u - U_p}{U - U_p} = \frac{1}{2}$. Equation 36 is plotted in Figure 17 for various values of n and is compared with experimental measurements.

D. Velocity Distribution in the Aft Part of the Ejector

If the ejector is long enough, the flow eventually becomes fully developed turbulent pipe flow. That is, after the mixing process of the primary and secondary flows in the inlet length of the mixing tube and the transition processes, a fluid particle will enter a flow regime where the velocity profile is unchanged with respect to the axial distance. This velocity profile can be expressed as a function of the radial coordinate

$$\left(\frac{u_2}{U_2} \right) = \left(\frac{z}{Re} \right)^{\frac{1}{m}}; \tag{38}$$

13

where $z = Re - \gamma$, and m is a function of the area ratio, μ , and the length ratio, L/D, or $\dfrac{L/D}{\mu}$

Experimental measurements and Equation 38 are compared in Figure 18. The variation of m with respect to $\dfrac{L/D}{\mu}$ is plotted in Figure 19.

14

DISCUSSION AND CONCLUSIONS

A. Discussion:

The experimental measurements for optimum thrust augmentation factor, velocity ratios, and pressure reduction ratios for the initial plane at various area ratios are compared with theory in Figures 12, 13, and 14. The discrepencies between experimental measurement and theory are smaller for the low area ratios than for the high area ratios. (Figure 12). This phenomenon can be explained as follows: frictional losses were neglected in deriving the formula, but in reality, skin friction losses were quite influential. For low area ratios, a shorter ejector was adequate to produce the optimum thrust augmentation factor; but for high area ratios, a longer ejector was needed. Consequently, frictional losses were larger for the high area ratios than for the low area ratios. The optimum thrust augmentation factor obtained in the present investigation was 1.50 when μ was 105.5.

Experimental results are compared with theory for the velocity ratios, α_1 , and α_2 , in Figure 13. The comparison between theory and experiments for the pressure variation with respect to area ratio is presented in Figure 14. The augmentation factor assumed its maximum value when the gap ratio was 0.8, as can be seen in Figure 10.

It seems reasonable to divide the flow field in the ejector into three regimes. (Figure 1). The first regime, where the mixing process of the free jet is almost retained, may be denoted as a modified free-mixing regime. Like the case of a free jet, a laminar core is attached to the exit of the nozzle. Unlike the case of a free jet, a potential flow parallel to the axis of the ejector surrounds the laminar core. A near discontinuity in velocity exists at the rim of the exit of the nozzle. This near discontinuity smoothes out downstream due to the viscous shearing stresses. The mixing zone "survives" the laminar core and the potential zone downstream, and eventually becomes fully developed turbulent pipe flow. (Figure 1). The wall boundary layer starts at the rim of the inlet of the ejector and continues to grow downstream. The edge of the wall boundary layer meets the boundary of the mixing zone at a location which can be computed theoretically or measured experimentally.

Theoretically, $\frac{X_m}{D}$ is 11.0 for μ = 16.0, 15.0 for μ = 29.6, 18.0 for μ = 46.7, and 32.6 for μ = 105.5. Experimentally, this location was found to be close to the theoretical location (Figure 15). $\frac{m}{D}$ is not only a function of the area ratio, but is also affected by the length ratio, L/De. Schiller, in his theory of inlet length flow of circular pipes, did not specify the length of the pipe; however, he implied that the pipe length was so great that the conditions at the inlet portion

15

was no longer a function of the length of the pipe. The ejectors of the present case were not long enough to fulfill the conditions in which Schiller's theory would be entirely applicable. The length of the ejector from the initial plane up to the location where the edge of the wall boundary layer joins the edge of the jet flow spread is denoted as the modified free-mixing flow regime.

As mentioned above, the flow field eventually becomes fully developed turbulent pipe flow if the ejector is long enough. A fully developed turbulent pipe flow, as denoted in this report, has a velocity profile which may be expressed by a fraction power formula,

$$\frac{U_z}{U_z} = \left(\frac{z}{Re}\right)^{\frac{1}{m}},$$

where m is a positive real number, z is the distance measured from the walls, and Re is the radius of the pipe.

The flow field in the ejector, after the potential flow vanishes and before the flow field becomes fully developed turbulent pipe flow, is denoted as the transition regime. The portion of the ejector, from the location where the velocity profile becomes that of a turbulent pipe flow to the end of the ejector, is denoted as the pipe flow regime. However, since the velocity profiles only asymptotically approached those of fully developed turbulent pipe flow, the length of the transition flow regime could not be distinctly defined.

The measured dimensions for the laminar core and mixing zone are compared with theory in Figure 16. The dimensions of a confined jet are quite different from those of a free jet (Reference 15). In the present case, the dimension of the laminar core is a function of the initial velocity ratio, α_1 ; consequently, it is a function of area ratio μ . There exists a close correlation between experiment and theory of these dimensions. (Figure 16). Also, Figure 16 shows close agreement between experiment and theory for the boundary of the mixing zone.

Measured potential velocity is compared with theory in Figure 11. The experimental results for the growth of the wall boundary layer are compared with theory in Figure 15. In these two figures, the axial distance was converted into the nondimensionalized product of ($\frac{x}{Re}$) and Reynolds number $\bar{R}, \left(\frac{Re\,U_1}{\nu}\right)$, where $\bar{R}$ was based on the radius of the ejector Re, and the induced secondary flow velocity U_1. In Figure 11, the potential velocity was plotted as the ratio of the difference between the local potential velocity, U_p, and the induced secondary velocity, U_1, to the induced secondary velocity, U_1.

The velocity profiles at different axial locations are shown in Figures 20-24 A comparison of the theoretical and experimental velocity profiles for $\mu = 29.6$ are shown in Figure 17 for the modified free-mixing flow regime. Unlike the case of a free jet flow, the value of n

16

not only varied wi in the range of 1.0 to 2.0, but exceeded 2.0 and approached 5.0, as can be seen in Figure 17e.

The centerline velocities for different area ratios are shown dimensionally in Figure 25. They are shown nondimensionally and compared with the centerline velocities for free jet flow in Figure 26. The centerline velocity for free jet flow is inversely proportional to the axial distance. (Reference 21). The inverse of the centerline velocity ratio, $\frac{U_o}{U}$, plotted against the axial distance ratio, $\frac{x}{D}$, shows a linear variation. (Figure 27). For the confined jets in this report, the experimental value of these quantities could be approximated by straight lines. The formulae representing the straight lines are shown in Figure 27. The slope of these lines, denoted by k, increases with area ratio, μ , as shown in Figure 28. As μ approaches infinity k tends toward 0.1362, which is the corresponding slope for a free jet. Therefore, the free jet flow might be interpreted as a confined jet flow with μ equal to infinity.

The velocity profiles at the outlets of the ejectors were measured and plotted nondimensionally in Figure 18. The data are compared with theory. It can be seen that the m values varied proportionally to the length ratio L/D, and inversely proportional to the area ratio, and that the m value varies proportionally to the ratio of the length ratio L/D to the area ratio μ , $\frac{L/D}{\mu}$. (Figure 19). This phenomenon is explained as follows: the ratio, $\frac{L/D}{\mu}$, could be interpreted as an indication of relative importance of the frictional forces in the flow field; i.e., skin frictional forces per unit momentum issued from the nozzle, and this ratio is the inverse of Reynolds Number based on significant variables to be determined. If the skin friction is relatively important, the velocity profile is fuller than that for a flow field where skin friction is not relatively important. The uncertainty raised herein is an interesting problem for future research.

Unlike the case of a free jet, the pressure was not constant in the flow field, as was measured and plotted in Figure 29.

B. Conclusions:

It is the author's belief that the mixing process within the ejector is an interchanging of momentum and energy among each stratum of the flow field. As soon as the ambient air is entrained into the ejector, the interchanging of momentum and energy occurs. Particles or groups of particles in the flow field which have possessed less momentum and energy will recieve some amount of external momentum and energy, and on the other hand, particles or groups of particles which are at higher energy and momentum level will lose some. It is beyond the scope of this report

17

to survey exactly the causes and consequences of this interchange of energy and momentum.

a. The Structure of the Flow Field in the Inlet Length of the Ejector.

1. The jet flow emerges at the exit of the nozzle as a constant velocity profile, and the secondary induced flow velocity is also constant throughout the rest of the cross section area at the initial plane. There is a near discontinuity of velocity at the rim of the exit of the nozzle. This near discontinuity in the velocity profile is smoothed gradually downstream.

2. A laminar core starts at the exit of the nozzle, and its radius decreases linearly with respect to the axial coordinate until it becomes a point on the longitudinal axis of the ejector. The length of the laminar core was about 6 nozzle diameters for the present experiment. Flow within the core is essentially uninfluenced by the confinement of the jet flow. The laminar core in the region of the turbulent-mixing flow can be described by the formula derived by Helmbold.

$$\frac{X_{js}}{R} = \frac{11.6}{1-\alpha_1} - 2.5(1-\alpha_1)$$

3. The jet flow starts mixing with the surrounding potential flow at the exit of the nozzle. The potential flow is uninfluenced by the viscous effects of the walls beyond the wall boundary layer. The mixing zone spreads outward linearly until it meets the boundary layer of the ejector. The radius of the mixing zone can be expressed as

$$\frac{Y}{R} = \frac{X/R}{\frac{11.6}{1-\alpha_1} - 2.5(1-\alpha_1)}\left[1.723 + 0.467(1-\alpha_1) + 0.25(1-\alpha_1)^2 - 1\right] + 1.$$

4. The wall boundary layer of the ejector is infinitely thin at the initial plane and it grows until meeting the boundary of the turbulent mixing zone. The growth of the wall boundary layer can be described in terms of potential flow velocity

$$\frac{\delta}{Re} = 2 - \sqrt{6\left(\frac{U_1 - U_P}{U_P}\right) + 4}.$$

5. The velocity profile within the wall boundary layer of the ejector assumes the parabolic shape $\frac{U}{U_P} = 2\left(\frac{z}{\delta}\right) - \left(\frac{z}{\delta}\right)^2.$

18

6. Beyond the region of turbulent mixing the potential flow velocity can be described by the following equation:

$$\frac{X}{Re} = \frac{1}{4}\overline{R}\, f(n)$$

7. The velocity profile within the turbulent-mixing region can be expressed by Cornish's extension of Cole's two-dimensional wake law,

$$\frac{u-U_P}{U-U_P} = \frac{1}{2}\left[1 - \cos\pi\left\{1-\left(1-(0.5)^{\frac{1}{n}}\right)\frac{w}{w_{\frac{1}{2}}}\right\}^{n}\right],$$

where n varies from 1.0 to 5.0 beyond the core region and up to the location where the boundary of the turbulent mixing meets the edge of the boundary layer of the walls. For this equation to be applicable beyond the laminar core region, w has to be changed to r and $w_{\frac{1}{2}}$ to $r_{\frac{1}{2}}$.

b. Centerline Velocity of the Ejector.

Centerline velocity is inversely proportional to the axial distance and can be expressed as

$$\frac{U}{U_0} = \frac{1}{CONSTANT + k\left(\frac{X}{D}\right)},$$

for each value of area ratio.

c. Velocity Profile at the Outlet of the Ejector.

Velocity profile at the outlet of the ejector can be expressed as

$$\frac{U_2}{U_2} = \left(\frac{z}{Re}\right)^{\frac{1}{m}},$$

where m is a positive real number.

d. Velocity Ratios and Augmentation Factor.

The augmentation factor, φ, and the velocity ratios, α_1 and α_2, can be expressed in terms of area ratio.

$$\alpha_1 = \frac{\sqrt{\left(\frac{81}{40}\right)^2 - \left[\frac{41}{20}\mu - \frac{1}{20}\right]\left[\frac{81}{80}\frac{1}{\mu}-1\right]} - \frac{81}{40}}{\left[\frac{41}{40}\mu - \frac{1}{40}\right]},$$

$$\alpha_2 = \frac{9}{8\mu}\left[1+(\mu-1)\frac{\sqrt{\left(\frac{81}{40}\right)^2-\left[\frac{41}{20}\mu-\frac{1}{20}\right]\left[\frac{81}{80}\frac{1}{\mu}-1\right]}-\frac{81}{40}}{\left[\frac{41}{40}\mu-\frac{1}{40}\right]}\right], \quad \varphi = \frac{4}{5}\mu\alpha_2^2.$$

For future research, it would be interesting to explore the characteristics of ar ejector with different primary and secondary fluids with different temperature ratios. It would also be very useful to study the characteristics of this arrangement under dynamic conditions; i.e., with the secondary fluid flowing.

For simplification of design, future studies of the jet ejector flow should include the possibility of the characteristics of the device being a function of only one parameter.

BIBLIOGRAPHY

1. C·use, L. E. and Tontini, R., <u>Research on Coaxial Jet Mixing</u>, (General Dynamics, Convair, GD/C-62-354A), (November 1962).

2. Flugel, G., <u>The Design of Jet Pumps</u>, (National Advisory Committee for Aeronautics, T. M. No. 982), (July 1941).

3. Fox, N. L., <u>Analytical Solution for Gross Thrust Change</u>, (Douglas Company, Report No. SM-13881), (December 1950).

4. McClintock, F. A. and Hood, J. H., <u>Aircraft Ejector Performance</u>, (Journal of the Aeronautical Sciences, Vol. 13), (November 1946).

5. Reid, J., <u>The Effect of a Cylindrical Shroud on the Performance of a Stationary Convergent Nozzle</u>, (Royal Aircraft Establishment, Report Aero. 2559), (January 1962).

6. von Karman, T., <u>Theoretical Remarks on Thrust Augmentation</u>, (Reissner Anniversary Volume, J. W. Edwards, Ann Arbor, Michigan), (1949).

7. Rabenneck, G. I., Shumpert, P. K., and Sutton, J. F., <u>Steady Flow Ejector Research Program</u>, (Lockheed), (December 1960).

8. Keenan, J. H., Neumann, E. P., and Lustwerk, F., <u>An Investigation of Ejector Design by Analysis and Experiment</u>, (MIT Guided Missiles Program), (June 1948).

9. Lockwood, R. M., <u>Investigation of the Process of Energy Transfer From an Intermittent Jet to an Ambient Fluid - Summary Report</u>, (Hiller Aircraft Corp., Report No. ARD-238), (June 1959).

10. Wells, W. G., <u>Theoretical and Experimental Investigation of a High Performance Jet Pump Utilizing Boundary Layer Control</u>, (Mississippi State University, Aerophysics Department, Research Report No. 30), (June 1960).

11. Wagner, F. and McCune, C. J., <u>A Progress Report on Jet Pump Research</u>, (University of Wichita, Engineering Report No. 085), (October 1952).

12. Wood, R. D., <u>Theoretical Ejector Performance and Comparison With Experimental Results</u>, (Wadc TR 54-556), (August 1954).

13. Cornish, J. J., <u>A Universal Description of Turbulent Boundary Layer Profiles With or Without Transpiration</u>, (Mississippi State University, Aerophysics Department, Research Report No. 29), (June 1960).

14. Kuethe, A. M., <u>Investigation of the Turbulent Mixing Regions Formed by Jets</u>, (Journal of Applied Mechanics, Vol. 2, No. 3), (September 1935).

15. Faris, G. N., <u>Some Entrainment Properties of a ˉ bulent Axi-Symmetric Jet</u>, (Mississippi S ate University, Aerophysic. ь ,artment, Research Report No. 39), (January 1963).

16. Tollmien, W., <u>Calculation of Turbulent Expansion Processes</u>, (National Advisory Committee of Aeronautics TM 1085), (September 1945).

17. Davies, P. O. A. L., Barrett, M. J., and Fisher, M. J., <u>Turbulence in the Mixing Region of a Round Jet</u>, (Aeronautical Research Council, ARC 23728), (April 1962).

18. Pai, S. I., <u>Fluid Dynamics of Jets</u>, New York, D. Van Nostrand, 1954.

19. Eckert, E. R. G. and Drake, Robert K., <u>Heat and Mass Transfer</u>, 2nd Edition, New York, McGraw-Hill, 1959.

20. Townsend, A. A., <u>The Structure of Turbulent Shear Flow</u>, Cambridge, 1956.

21. Schlichting, H., <u>Boundary Layer Theory</u>, 4th Edition, New York, McGraw-Hill, 1960.

22. Goldstein, S., <u>Modern Developments in Fluid Dynamics</u>, 2 volumes, Oxford, 1938.

23. Langhaar, H. L., <u>Steady Flow in the Transition Length of a Straight Tube</u>, (Journal of Applied Mechanics), (June 1942).

24. Schiller, L., <u>Die Entwicklung der Laminaren Geschwindigkeitsuerteilung und ihre Bedentung für Zähigkeitsmessungen</u>, (Zeitschrift für Angewandte Mathematik und Mechanik, 1922).

25. Talbot, L., <u>Laminar Swirling Pipe Flow</u>, (Journal of Applied Mechanics, Vol. 21), (1954).

26. Helmbold, H. B., <u>Contribution to Jet Pump Theory</u>, (University of Wichita Report No. 294), (September 1957).

27. Helmbold, H. B., Luessen, G., and Heinrich, A. M., <u>An Experimental Comparison of Constant-Pressure and Constant-Diameter Jet Pumps</u>, (University of Wichita, Engineering Report No. 147), (July 1954).

28. Helmbold, H. B., _Energy Transfer by Turbulent Mixing Under a Longitudinal Pressure Gradient._ (University of Wichita, Engineering Study 182), (August 1955).

29. Squire, H. B. and Trouncer, J., _Round Jet in a General Stream_, Cited in Reference 1.
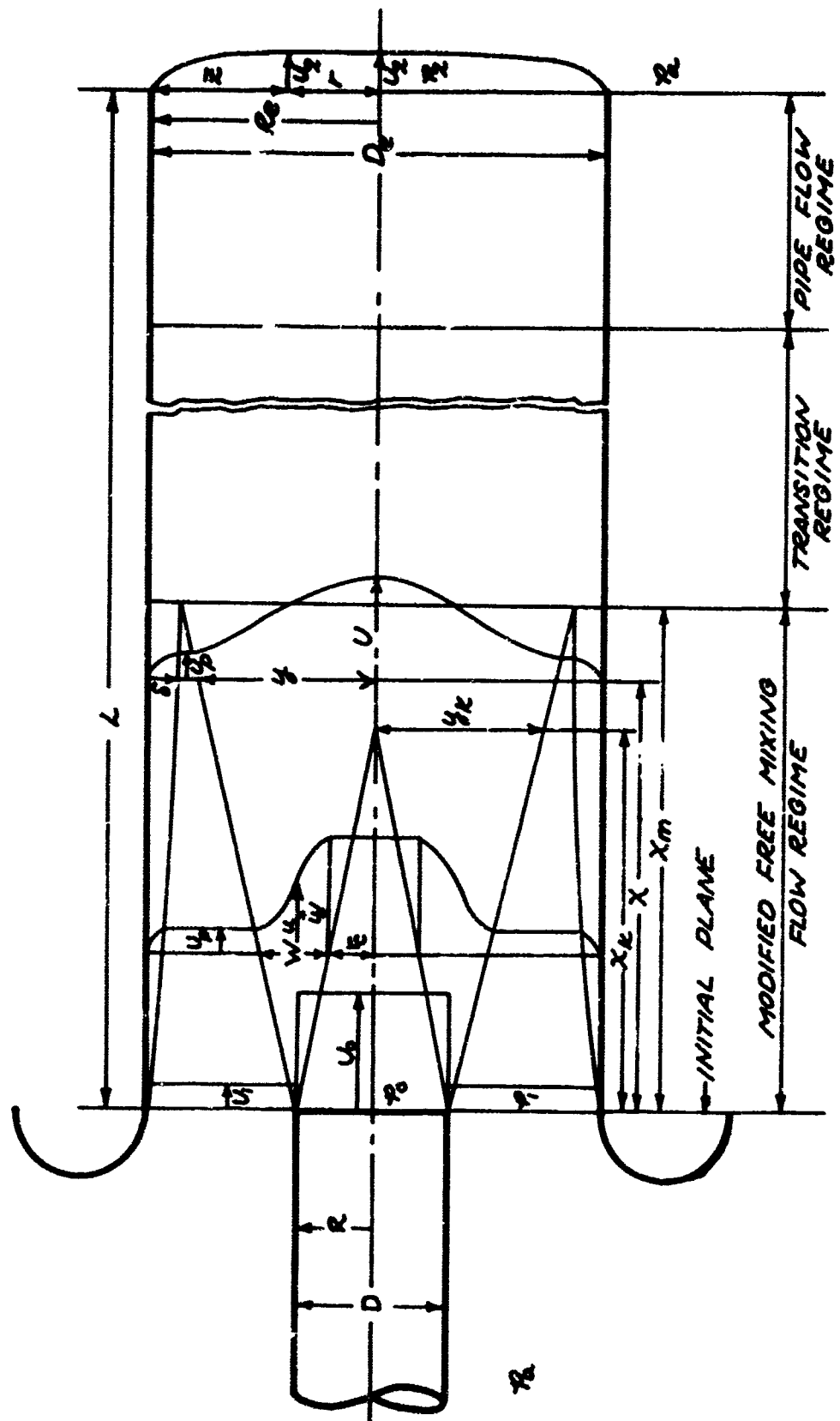
Figure 1. Jet Ejector, Nomenclature and Flow Regimes.

24
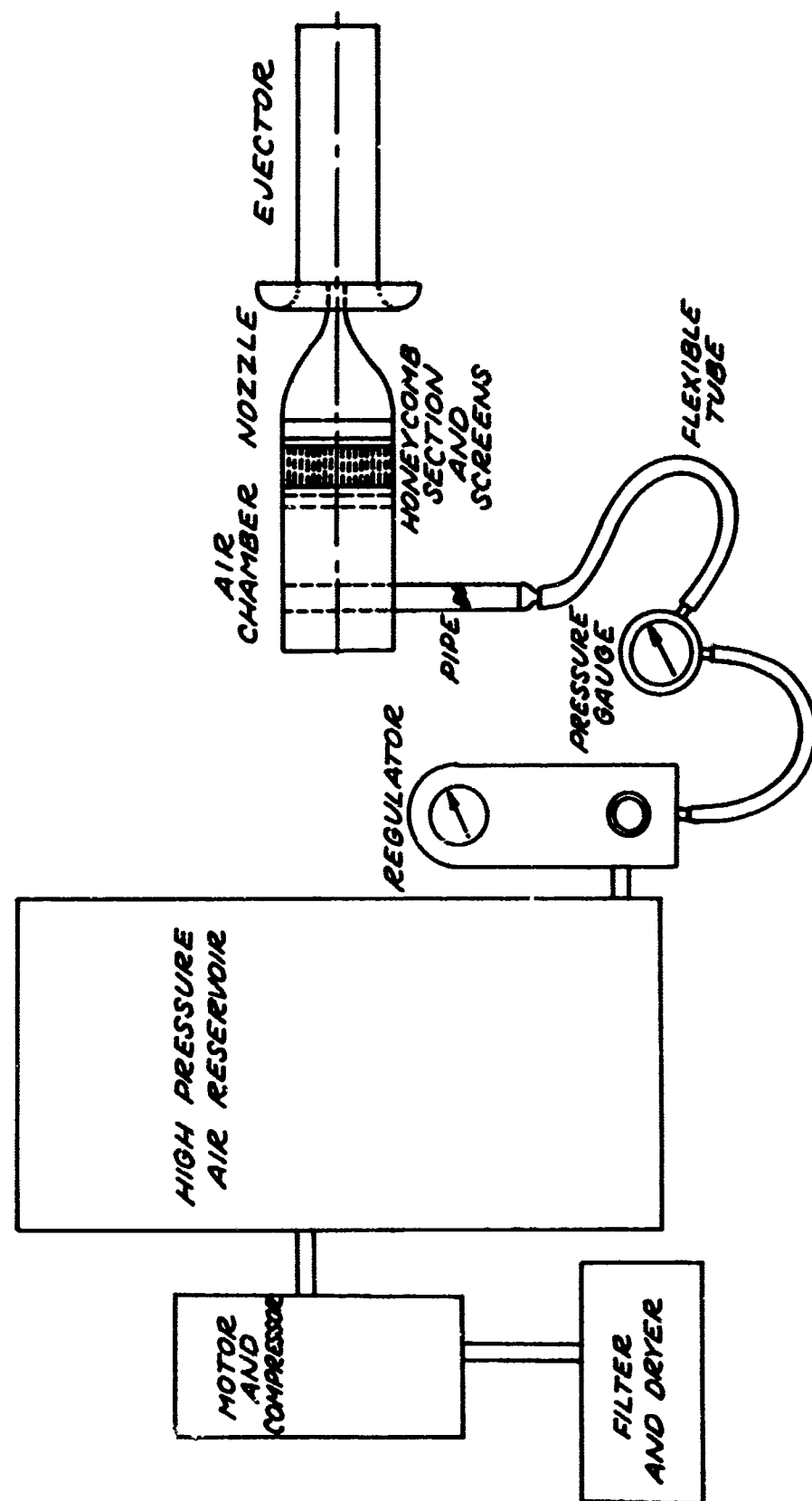
Figure 2. Descriptive Layout of Apparatus.

EJECTOR

AIR CHAMBER NOZZLE

HONEYCOMB SECTION AND SCREENS

FLEXIBLE TUBE

PIPE

PRESSURE GAUGE

REGULATOR

HIGH PRESSURE AIR RESERVOIR

MOTOR AND COMPRESSOR

FILTER AND DRYER

25
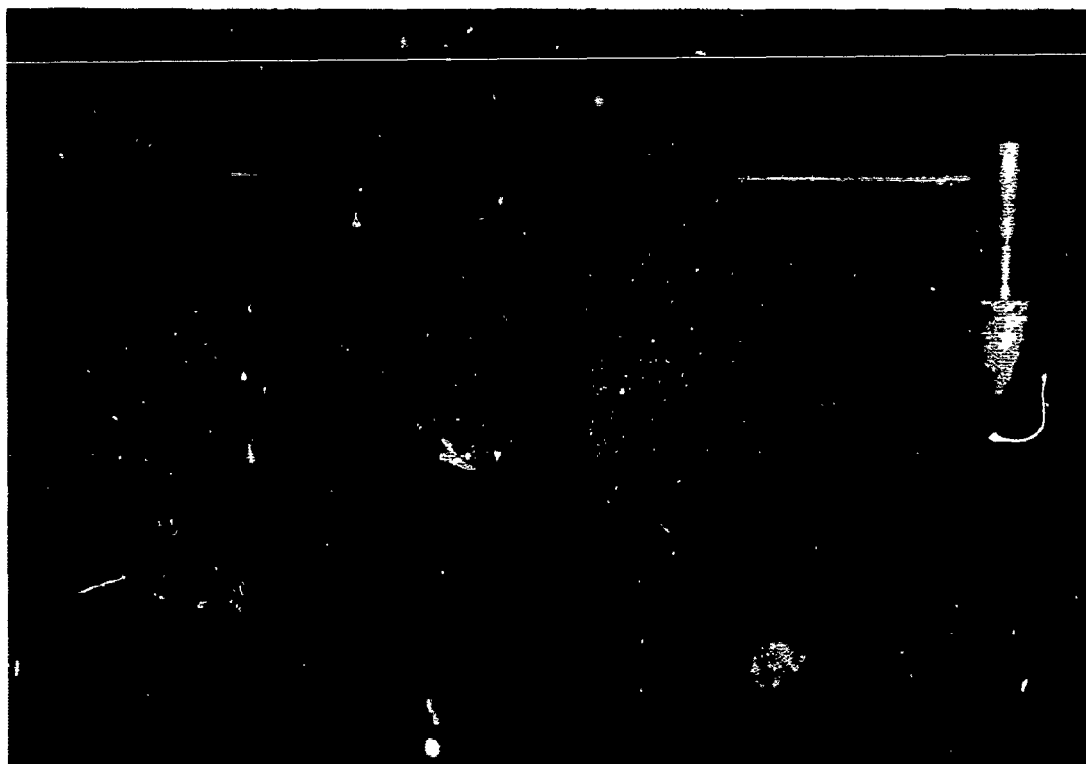
Figure 3a.   Thrust Force Measuring Unit.

Figure 3b.   Jet Flow Unit, Nozzle, and Supporting Rig.

26
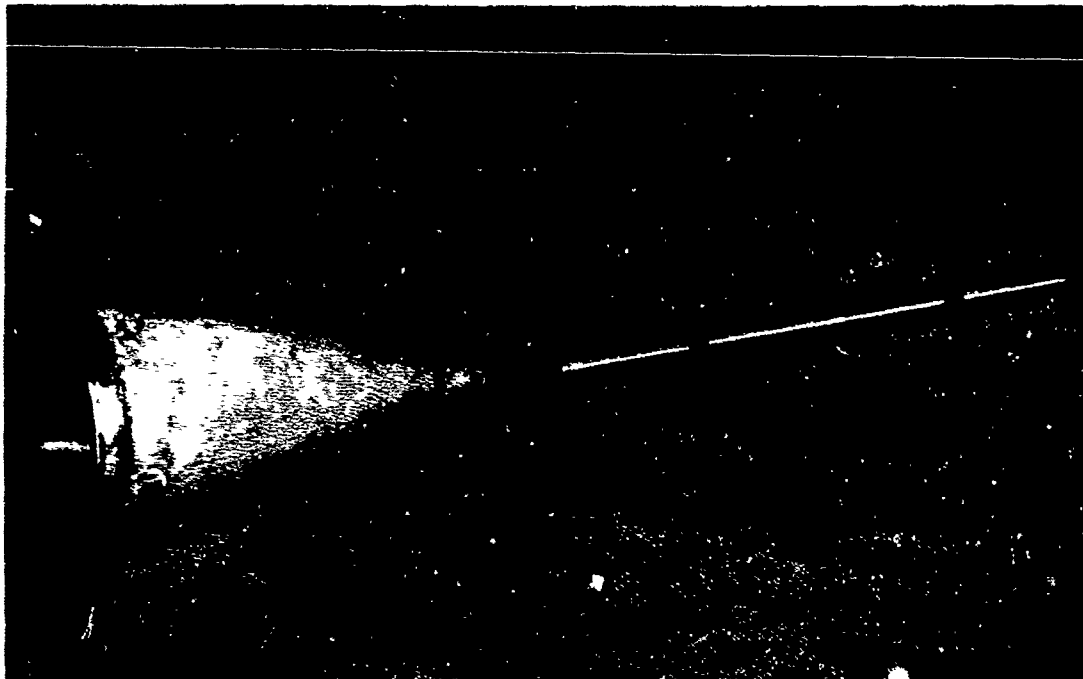
Figure 4. Extension for the Nozzle Exit.
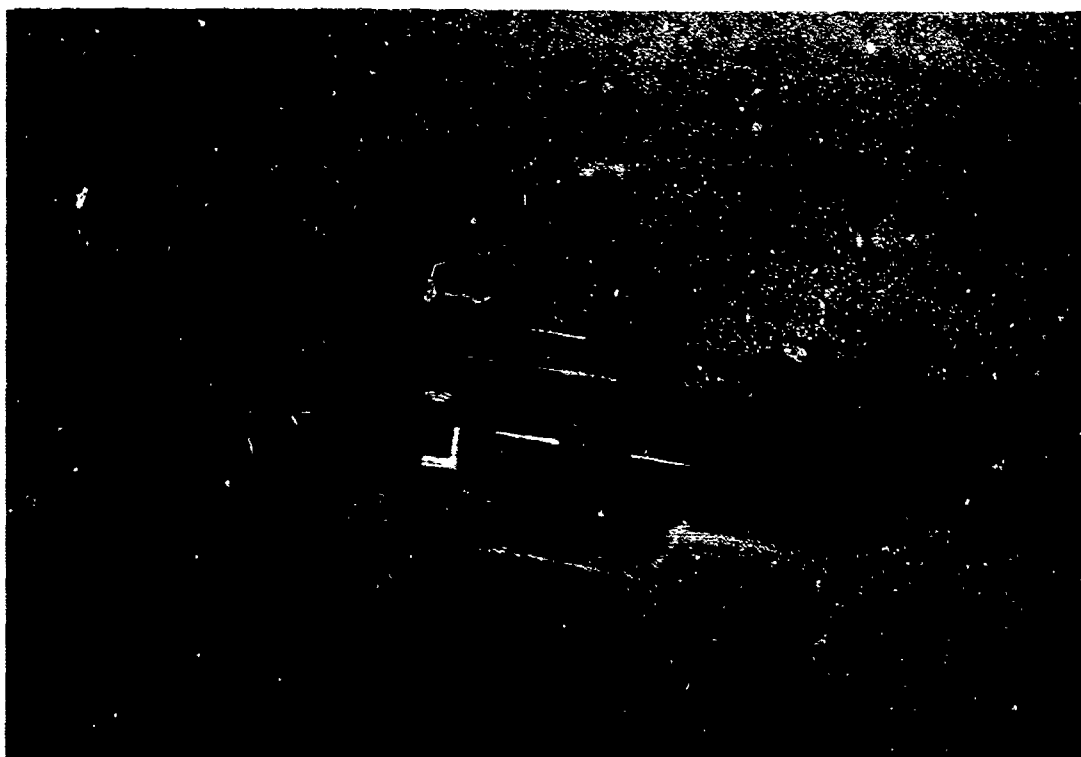
Figure 5. Pitot Tube Probe and Traversing Mechanism.

27
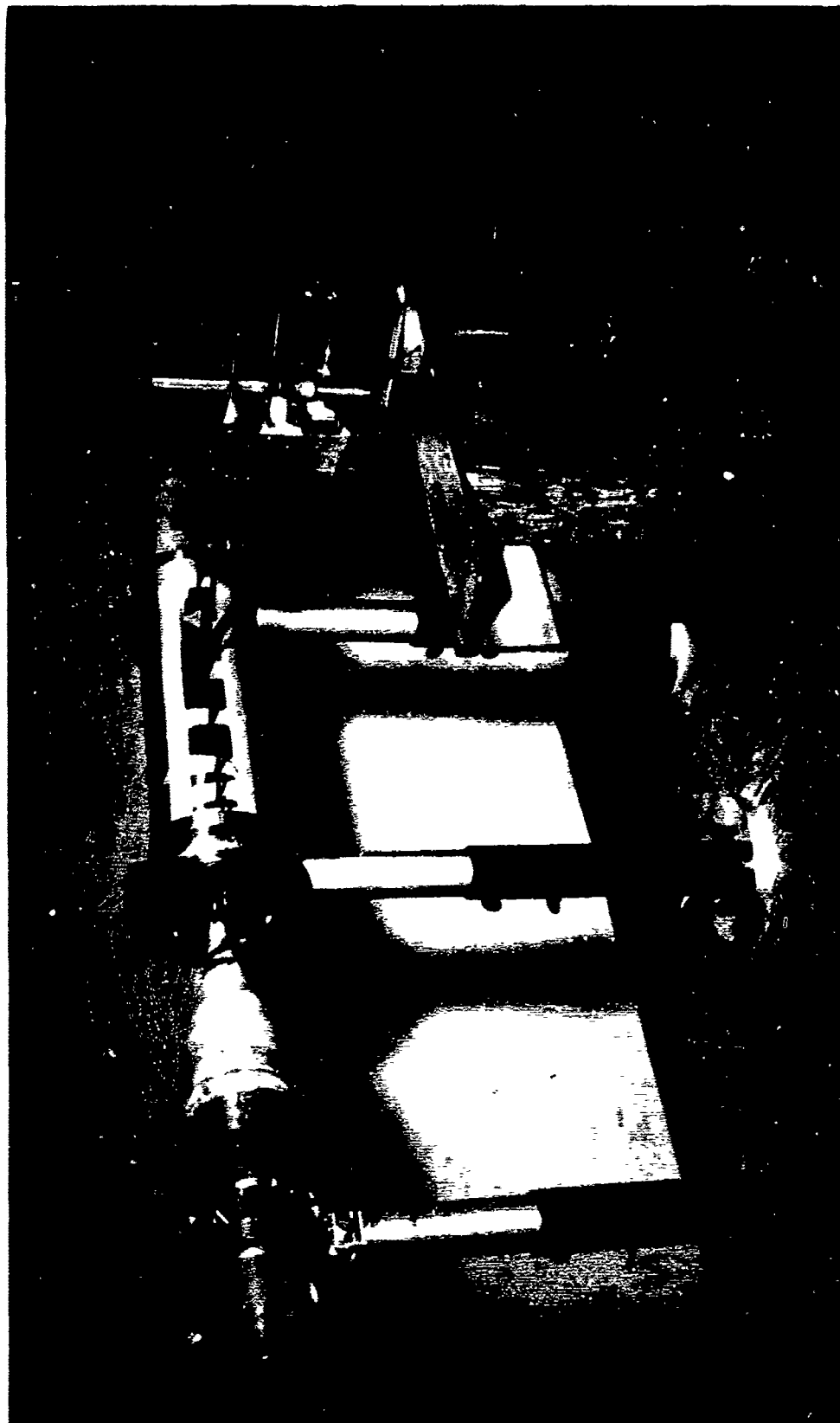
Figure 6. Velocity-Measuring Setup.
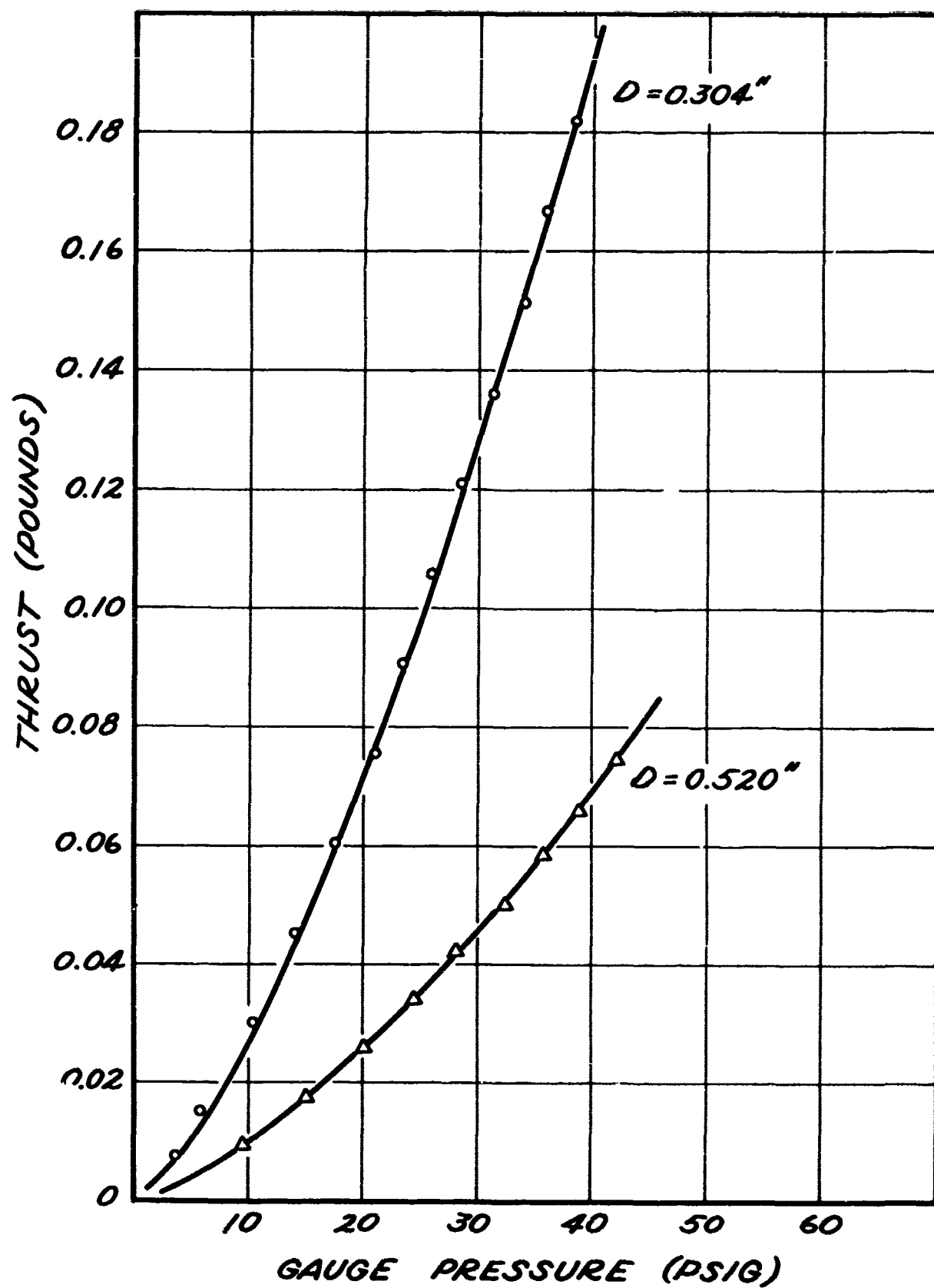
Figure 7.   Thrust Forces of Nozzles.
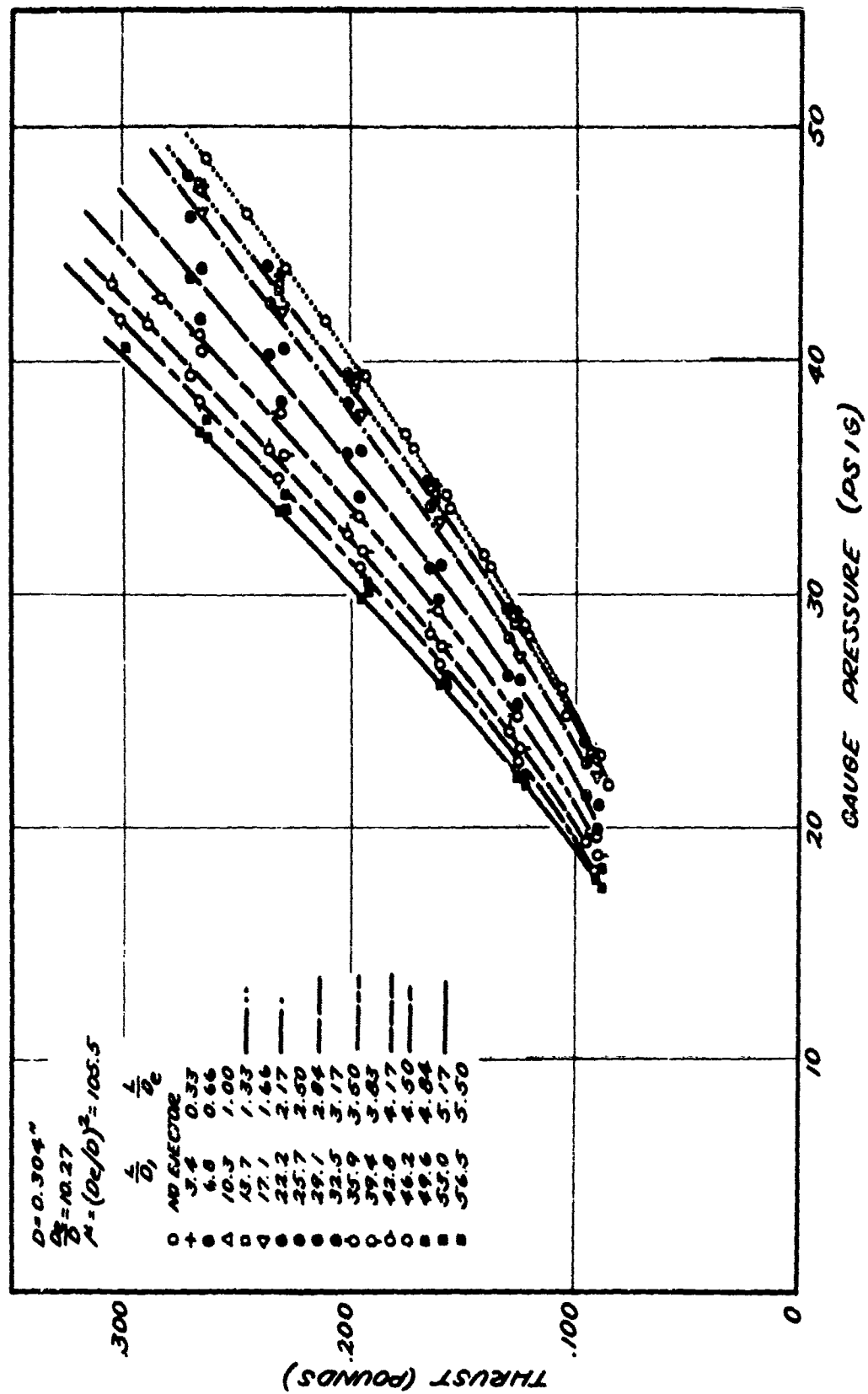
Figure 8. Thrust Forces of Jet Ejector μ = 105.5.
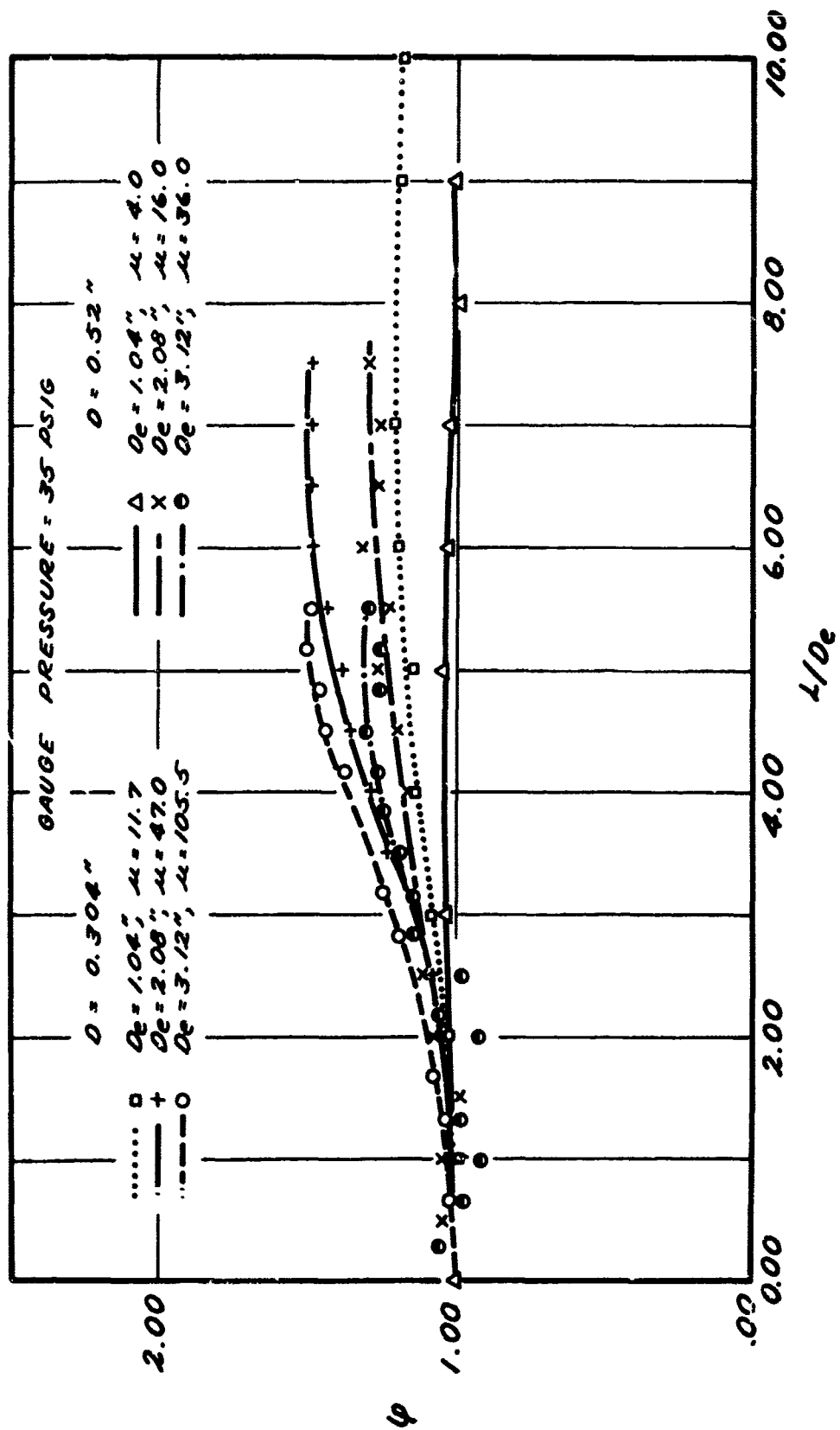
Figure 9. Effect of the Length Ratio on Augmentation Factor.
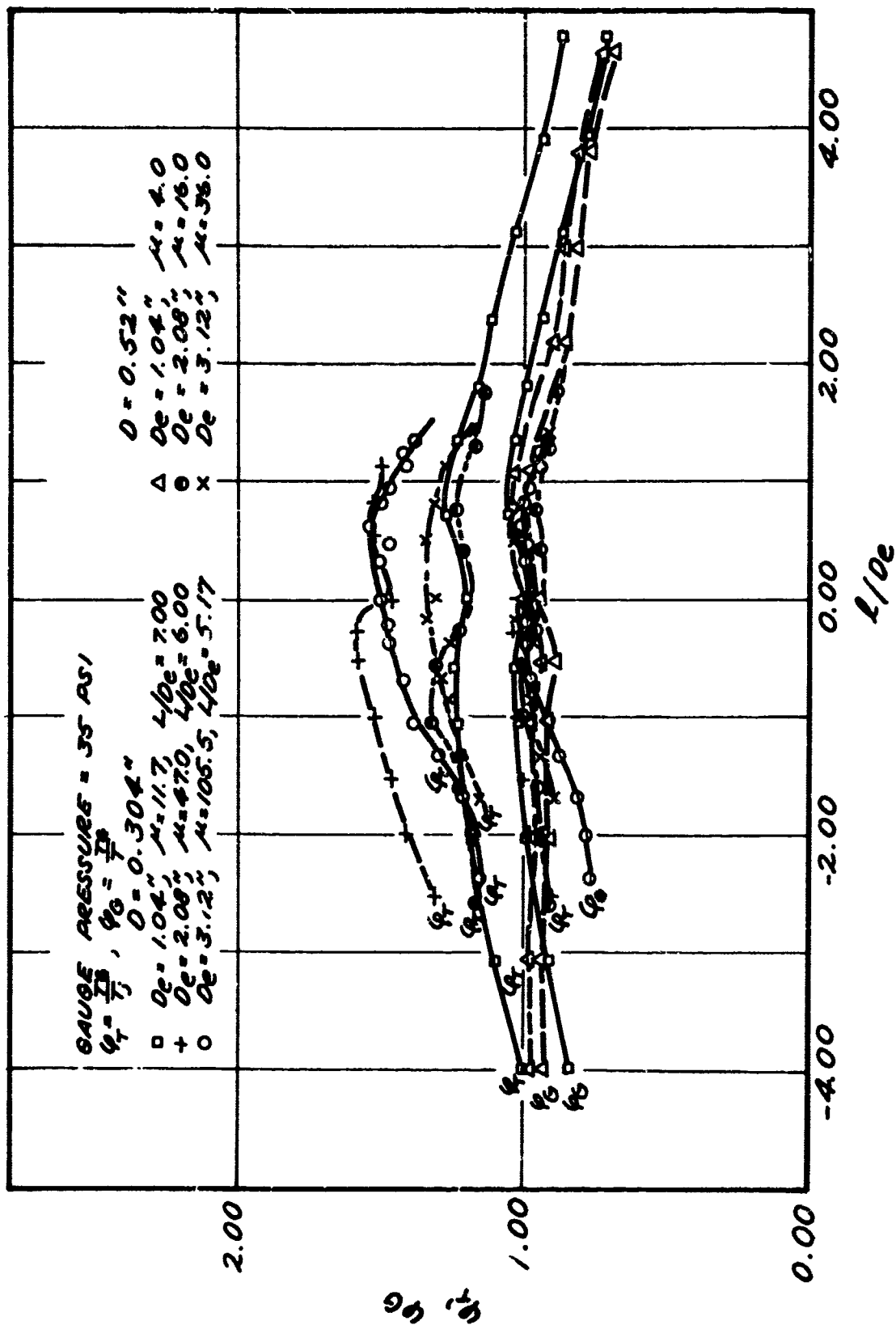
Figure 10. Effect of Gap Ratio on Augmentation Factor.

32
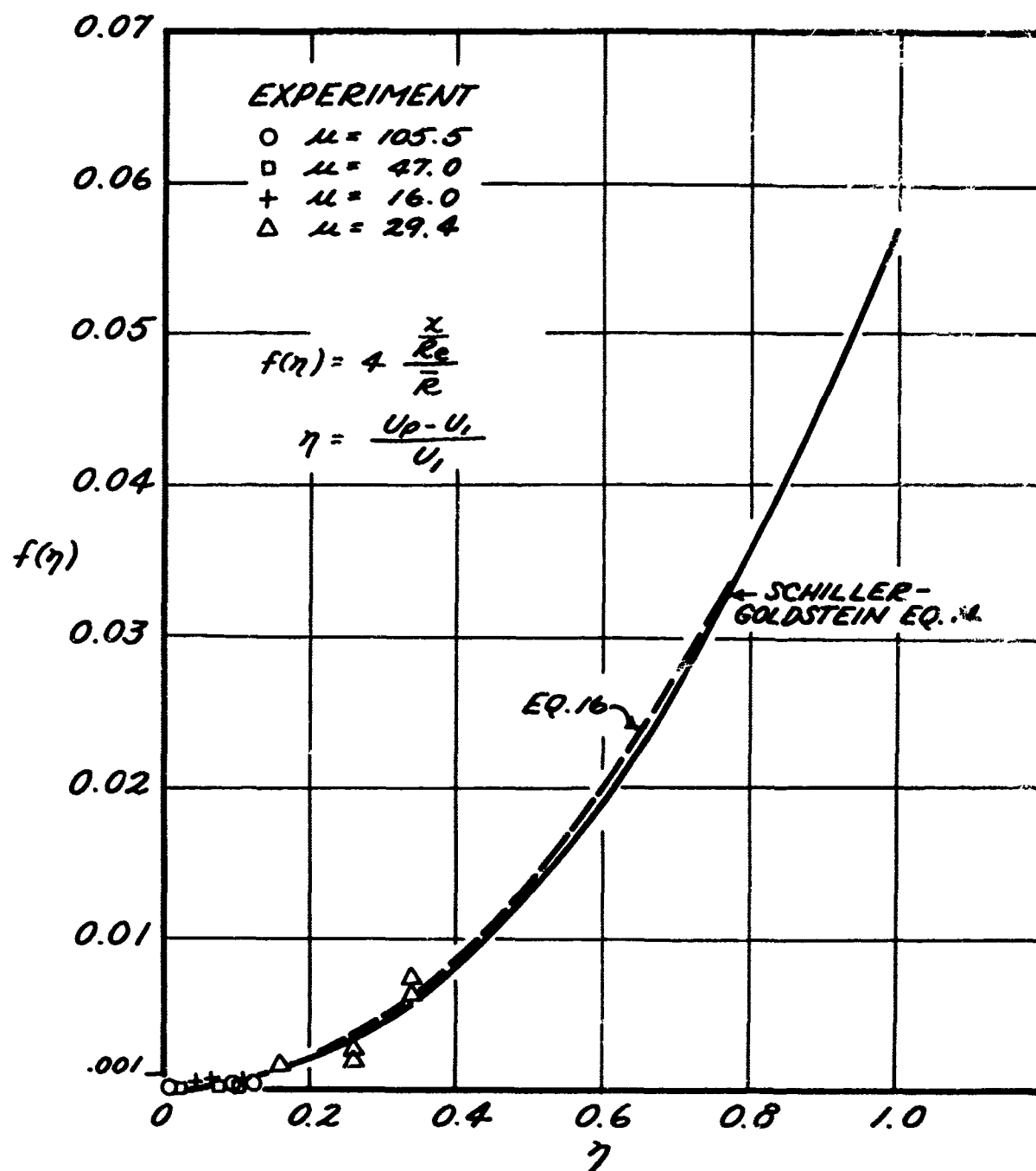
Figure 11. Comparison of Theoretical
and Experimental Potential Velocity.

33
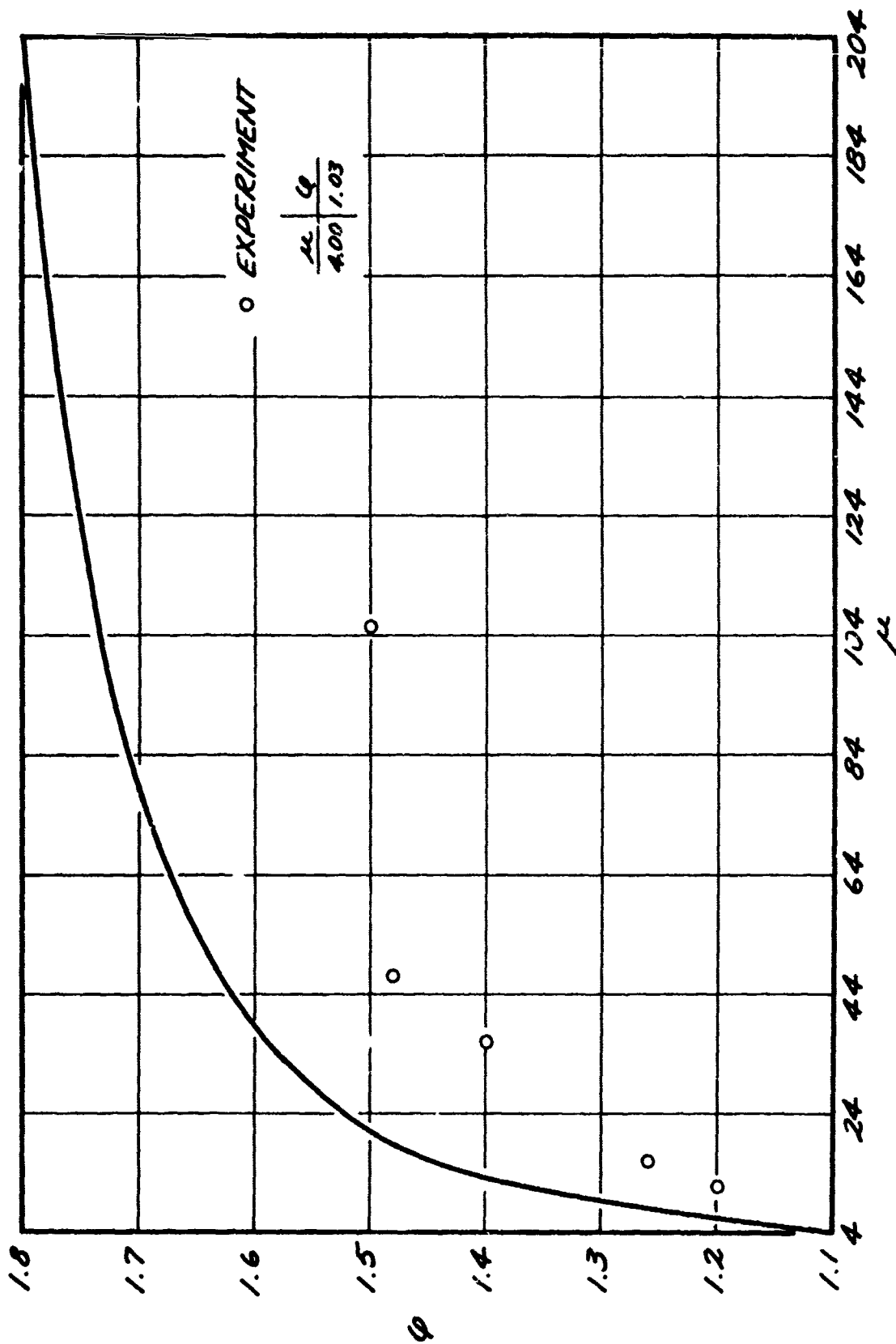
Figure 12. Comparison of Theoretical and Experimental Thrust Augmentation Factor.

34
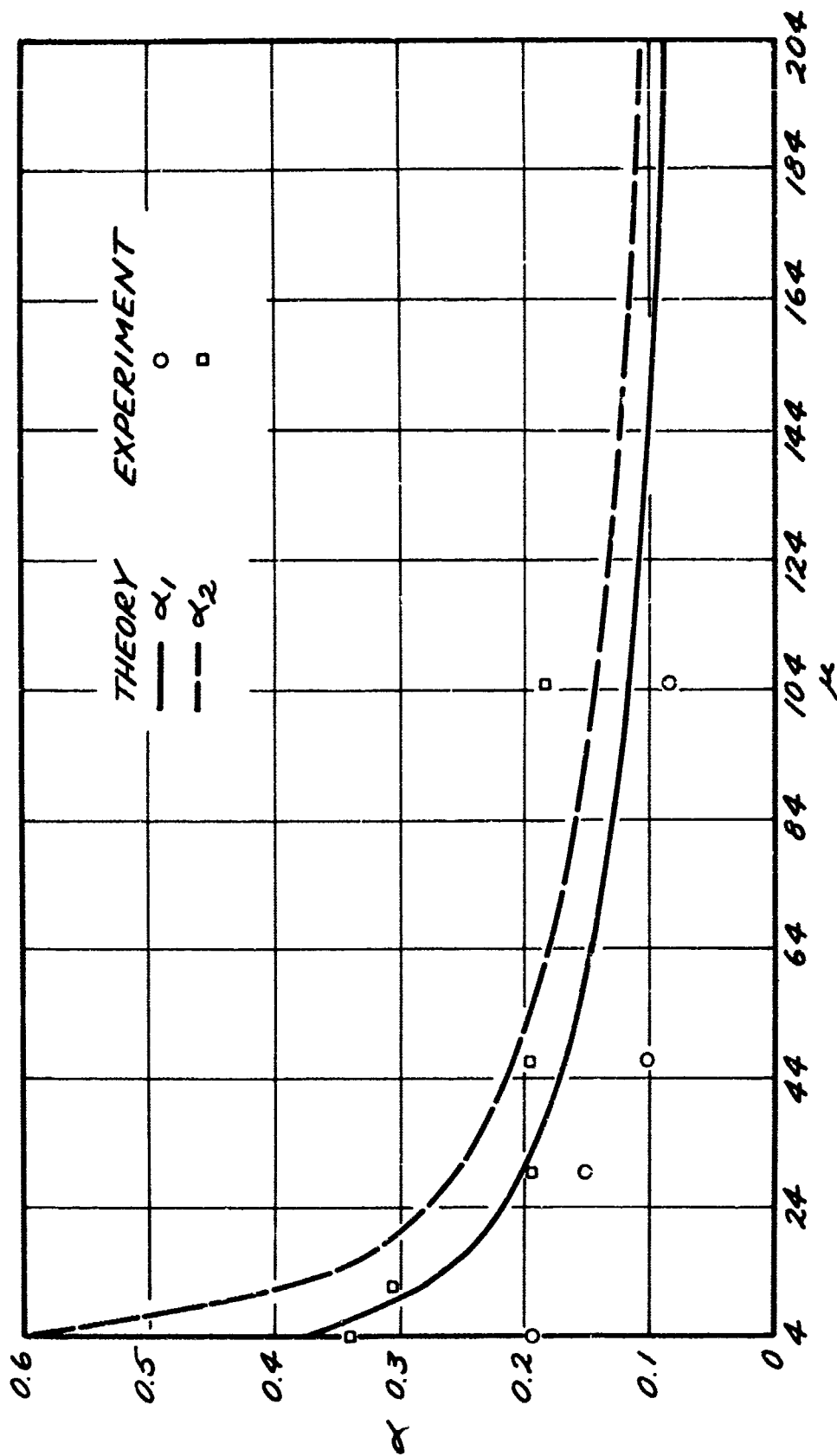
Figure 13. Comparison of Theoretical and Experimental Velocity Ratios.

35
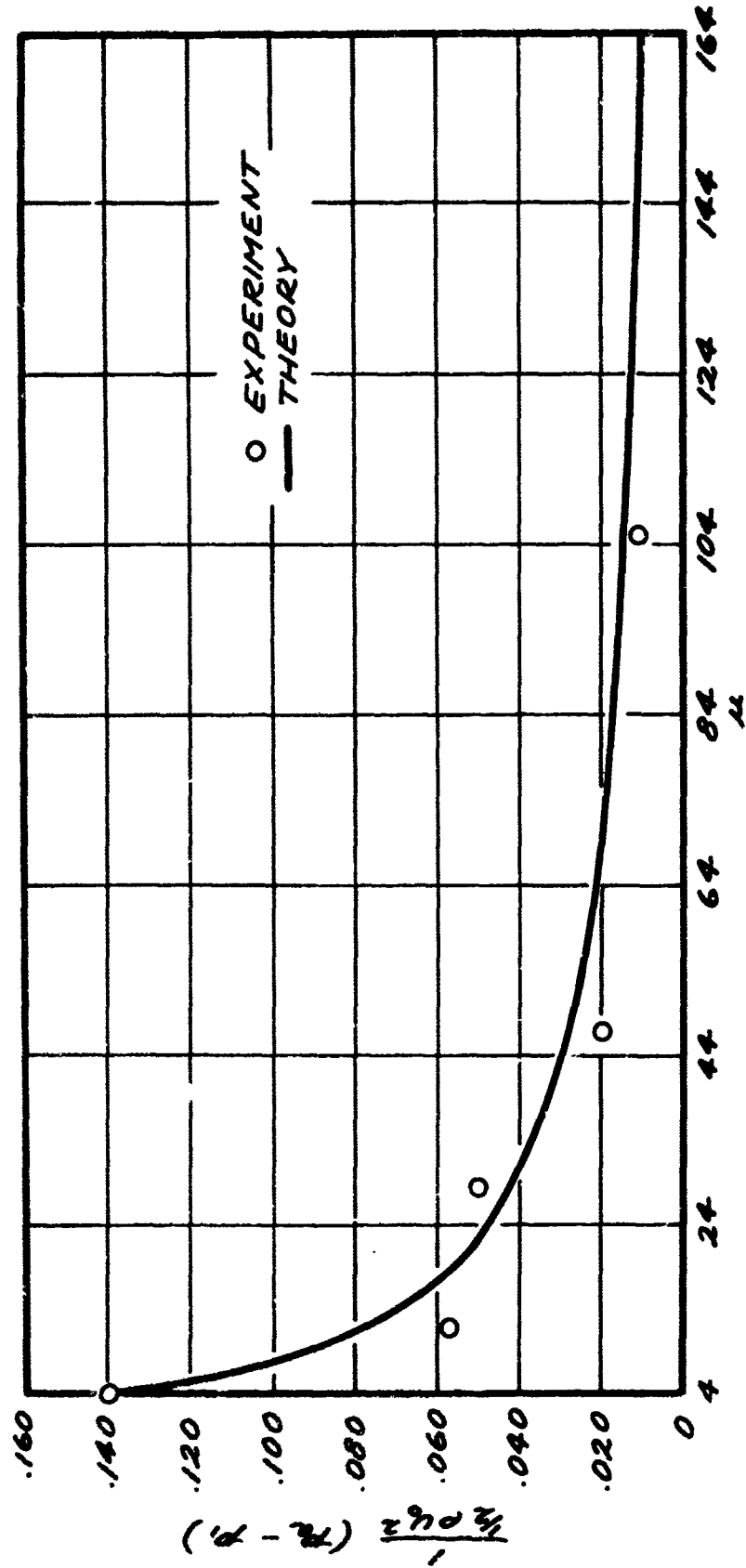
Figure 14. Comparison of Theoretical and Experimental Pressure Reduction Ratio at Initial Plane.
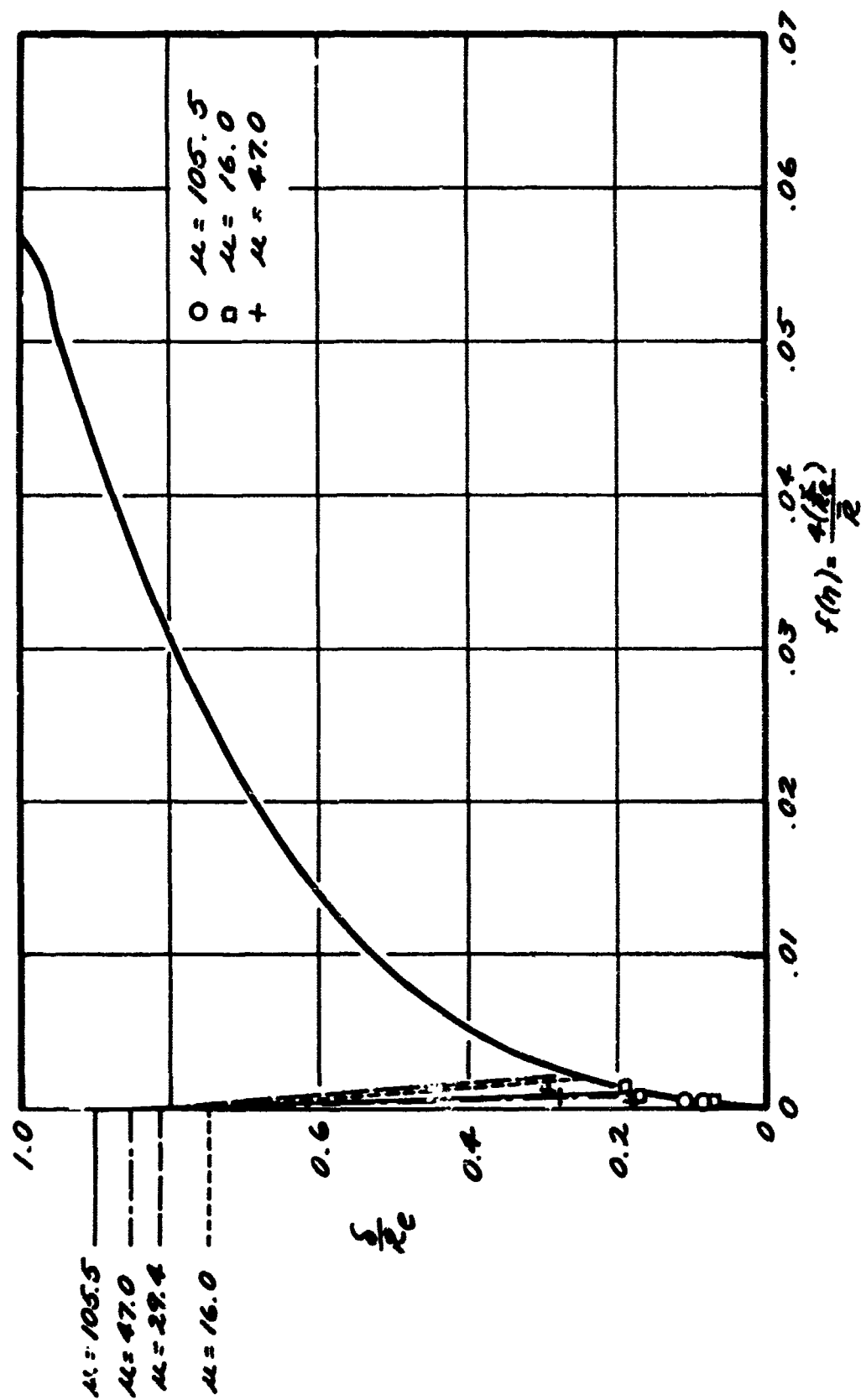
Figure 15. Theoretical Boundary of the Turbulent Mixing Zone and Comparison of Theoretical and Experimental Thickness of Boundary Layer of the Walls.

37
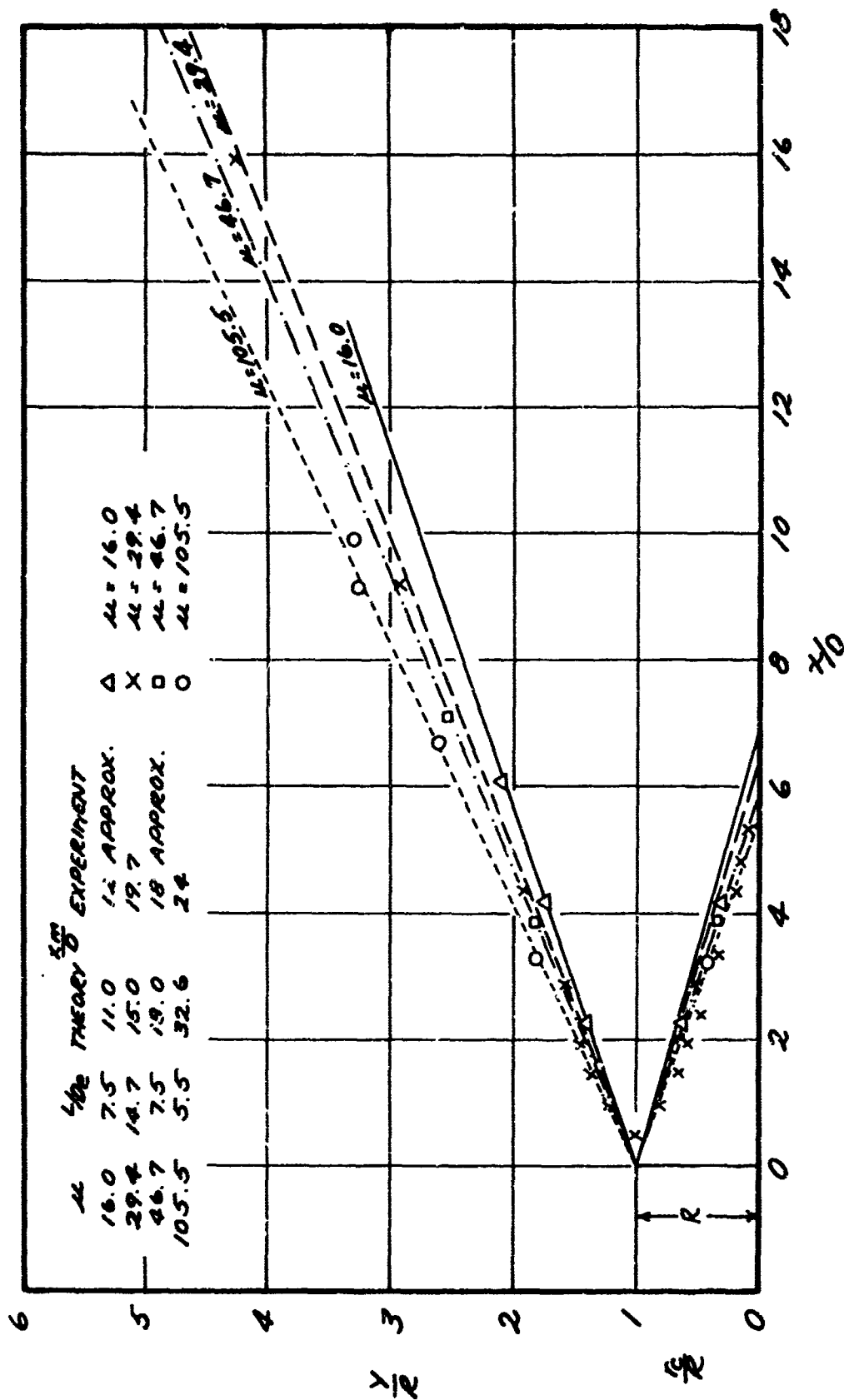
Figure 16. Comparison of Theoretical and Experimental Dimensions of Laminar Core and Turbulent Mixing Zone.
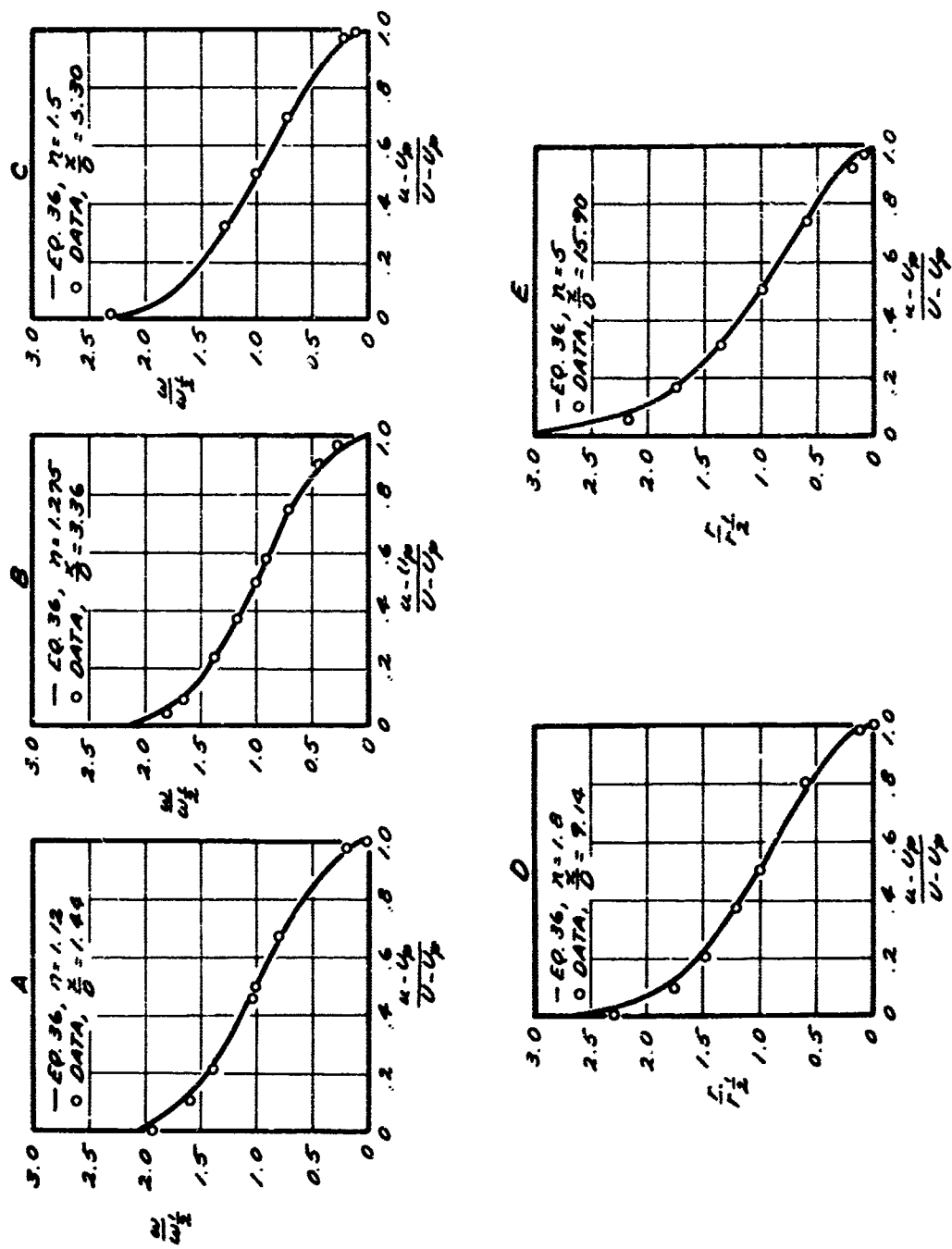
Figure 17. Comparison of Theoretical and Experimental Velocity Profiles in Inlet Length of Ejector, $\mu = 29.4$, $L/D_E = 150$.
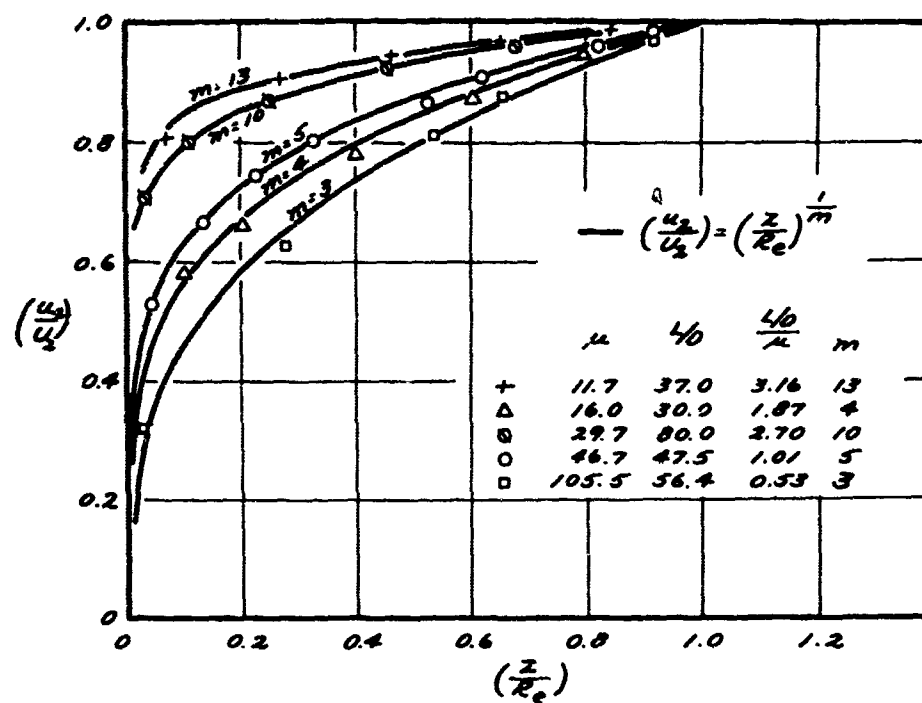
Figure 18.

Comparison of Theoretical and Experimental Velocity Profiles at Outlet of Ejector.
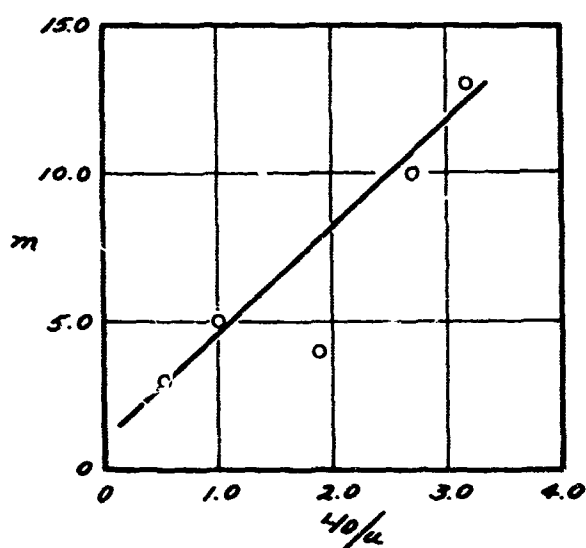
Figure 19. Effect of $\frac{L/D}{\mu}$ on m.

40
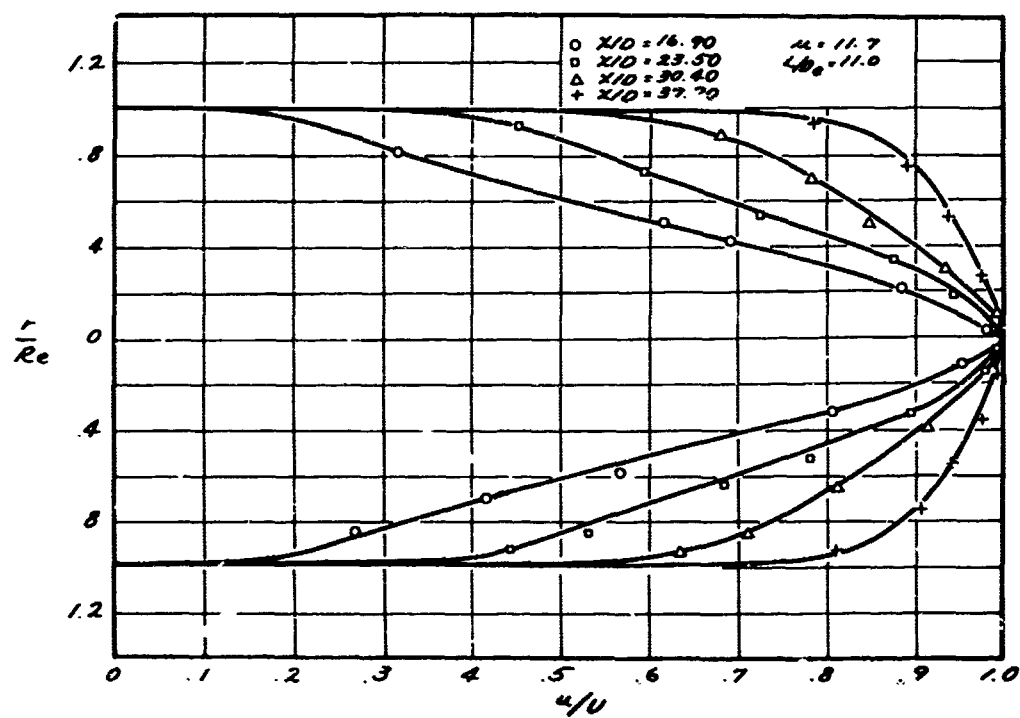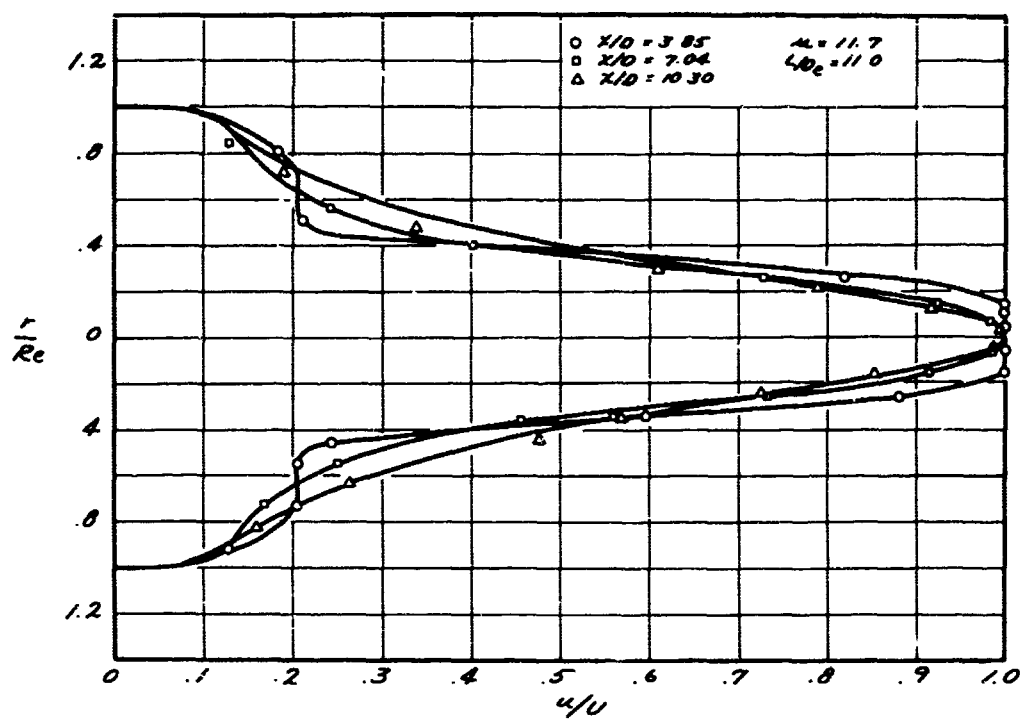
Figure 20.   Velocity Profiles, μ = 11.7.

41
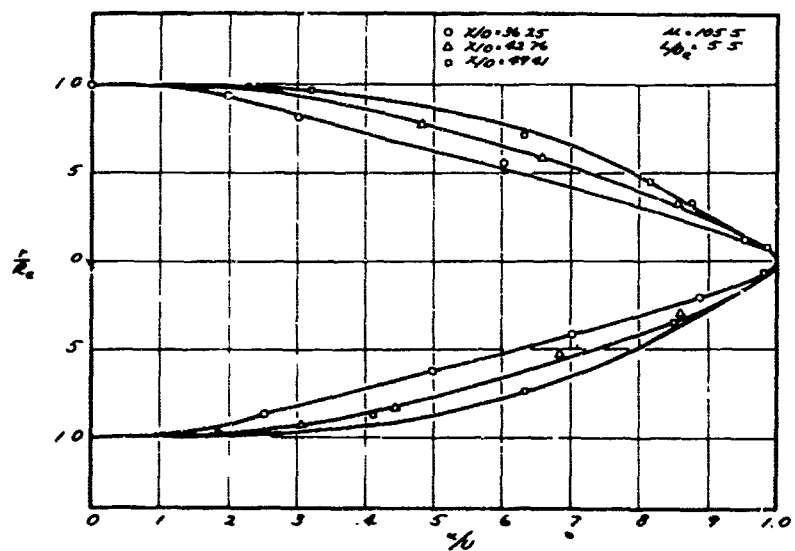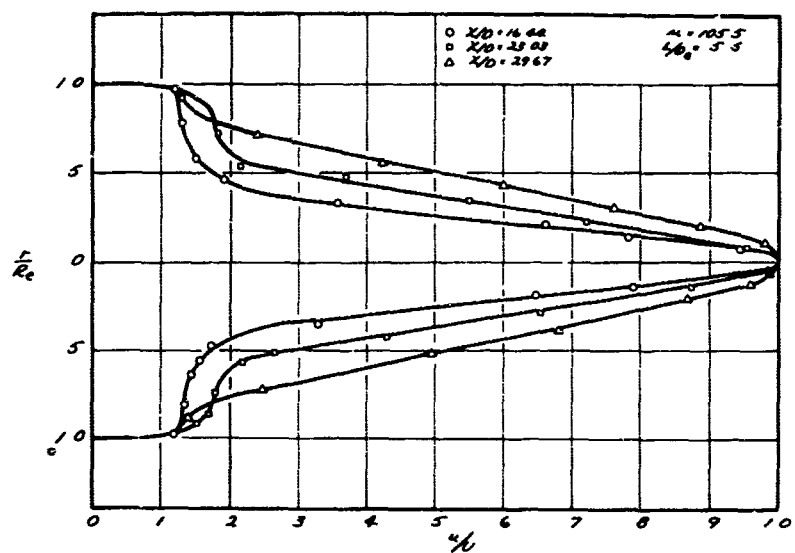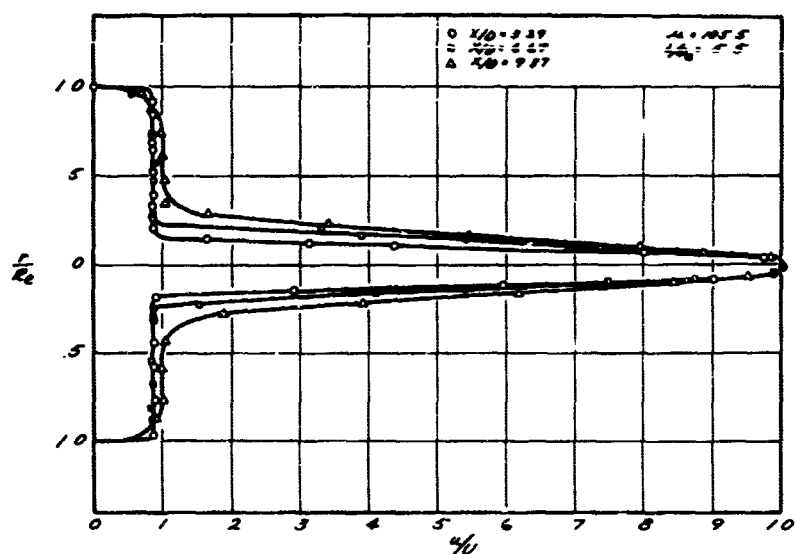
Figure 21. Velocity Profiles, μ = 16.0.
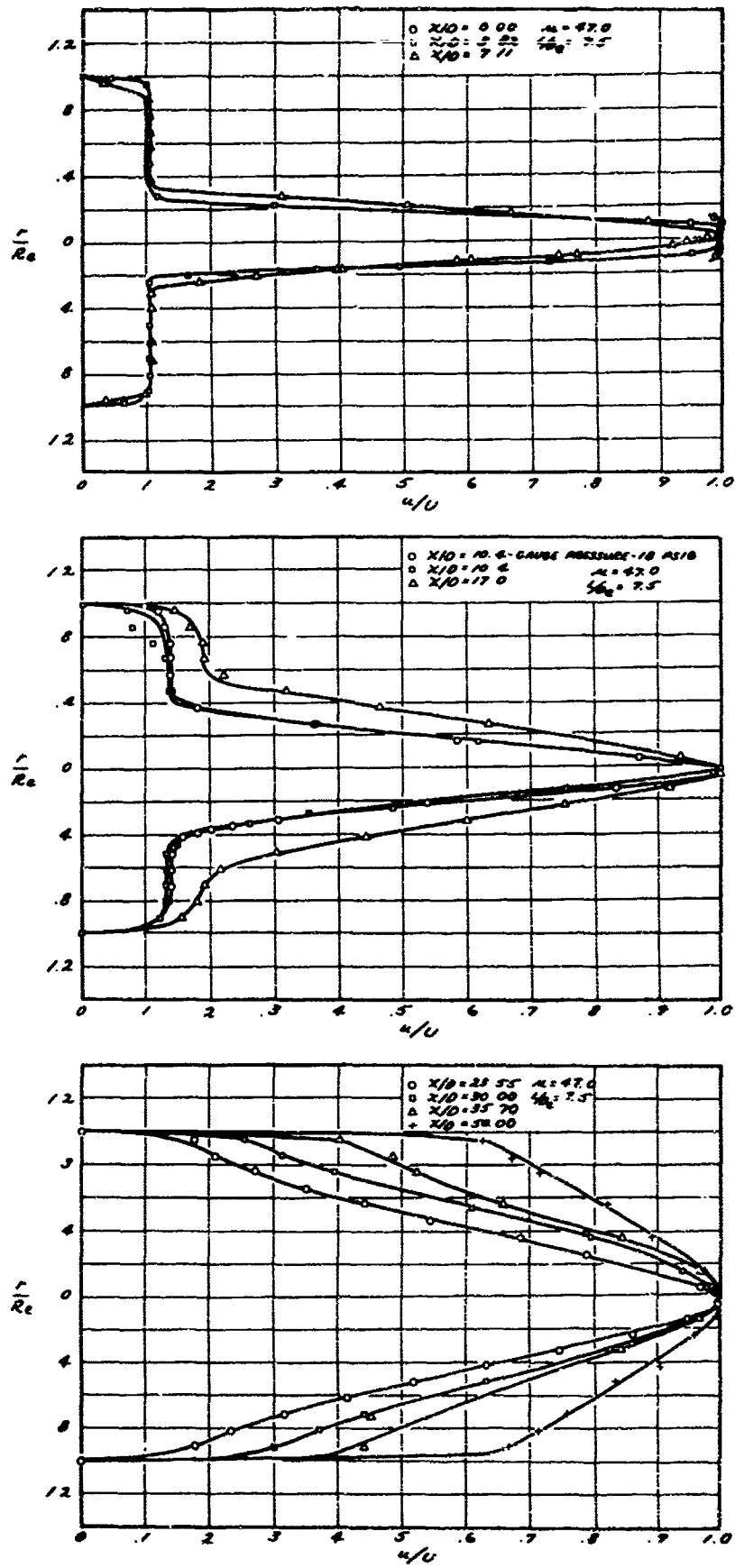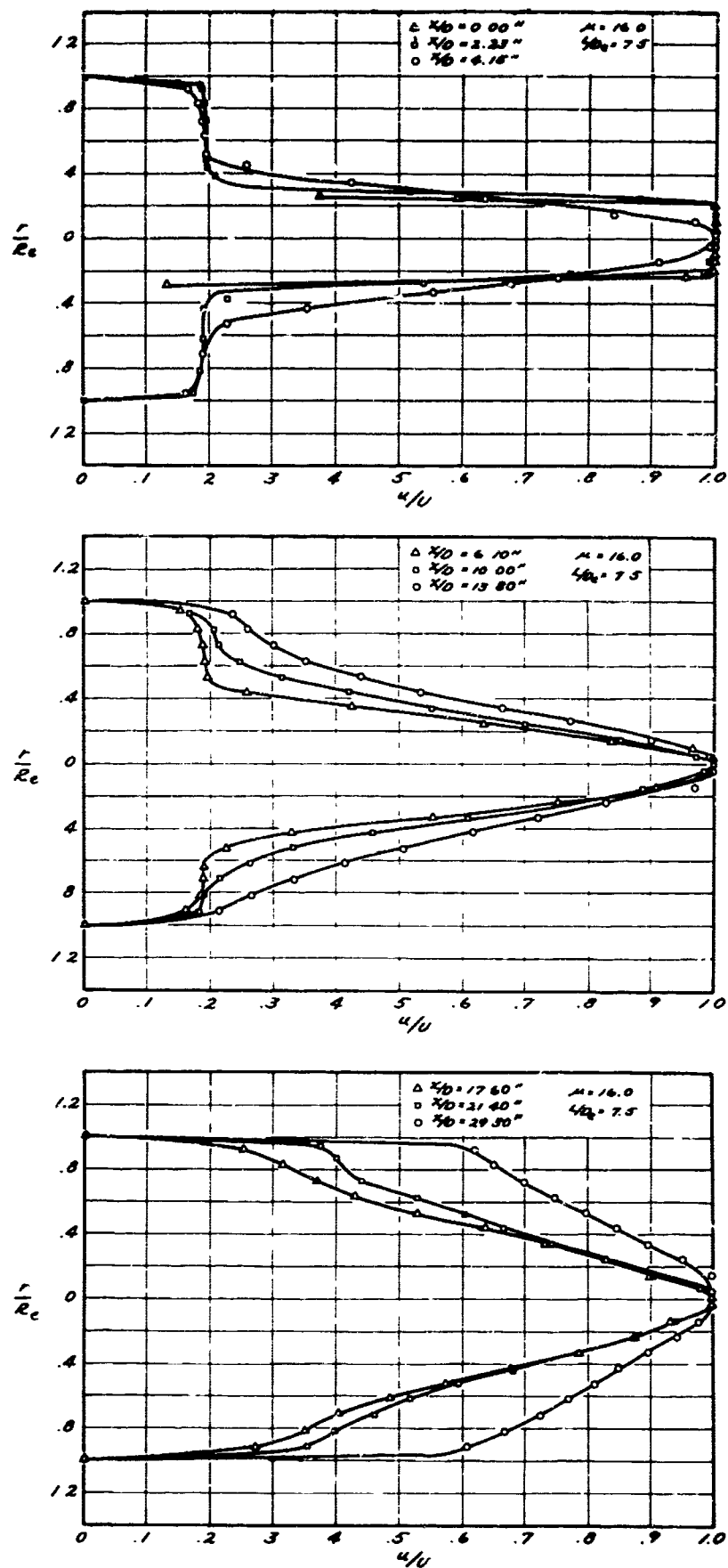
Figure 22. Velocity P_ofiles, μ = 47.0.

43

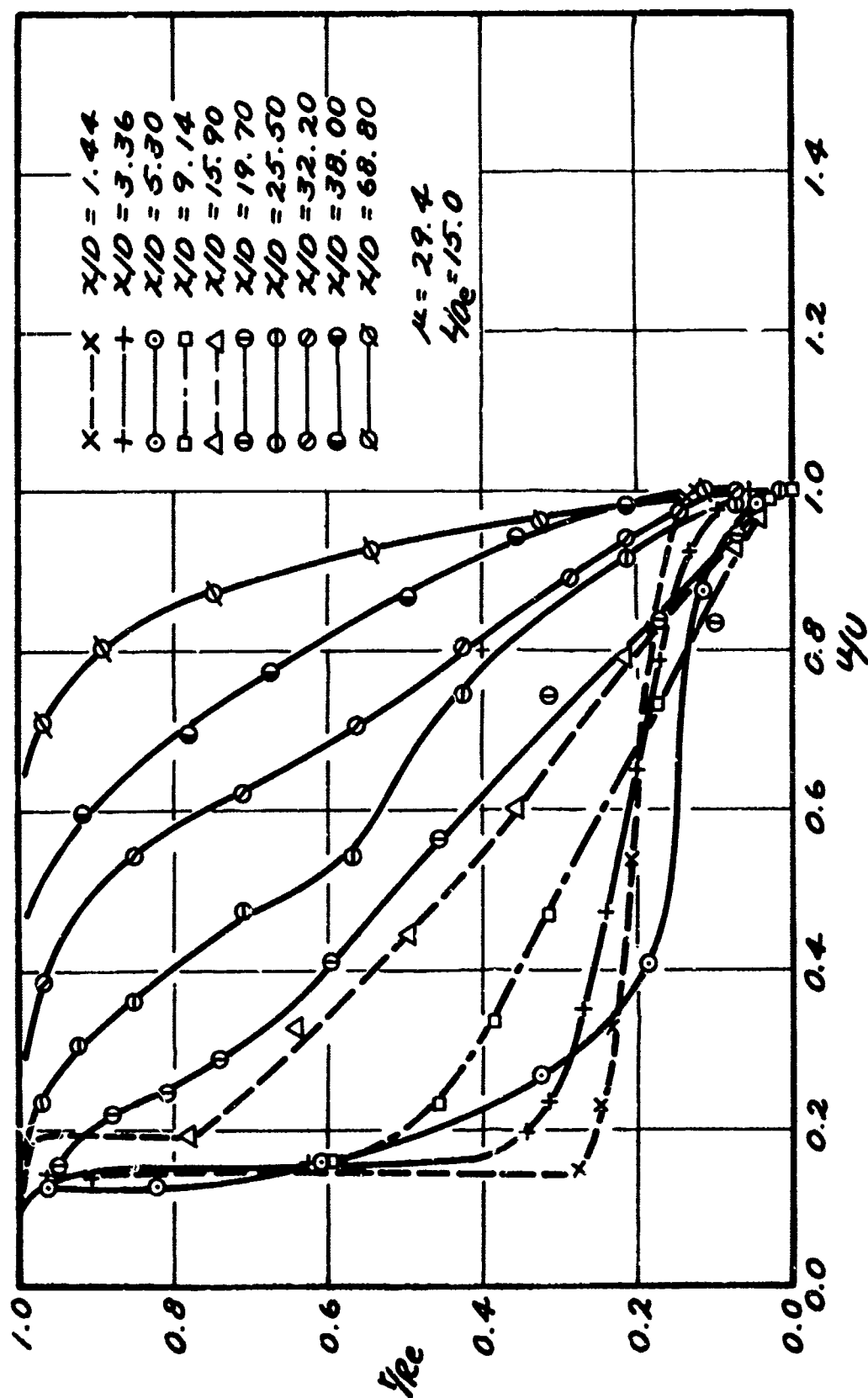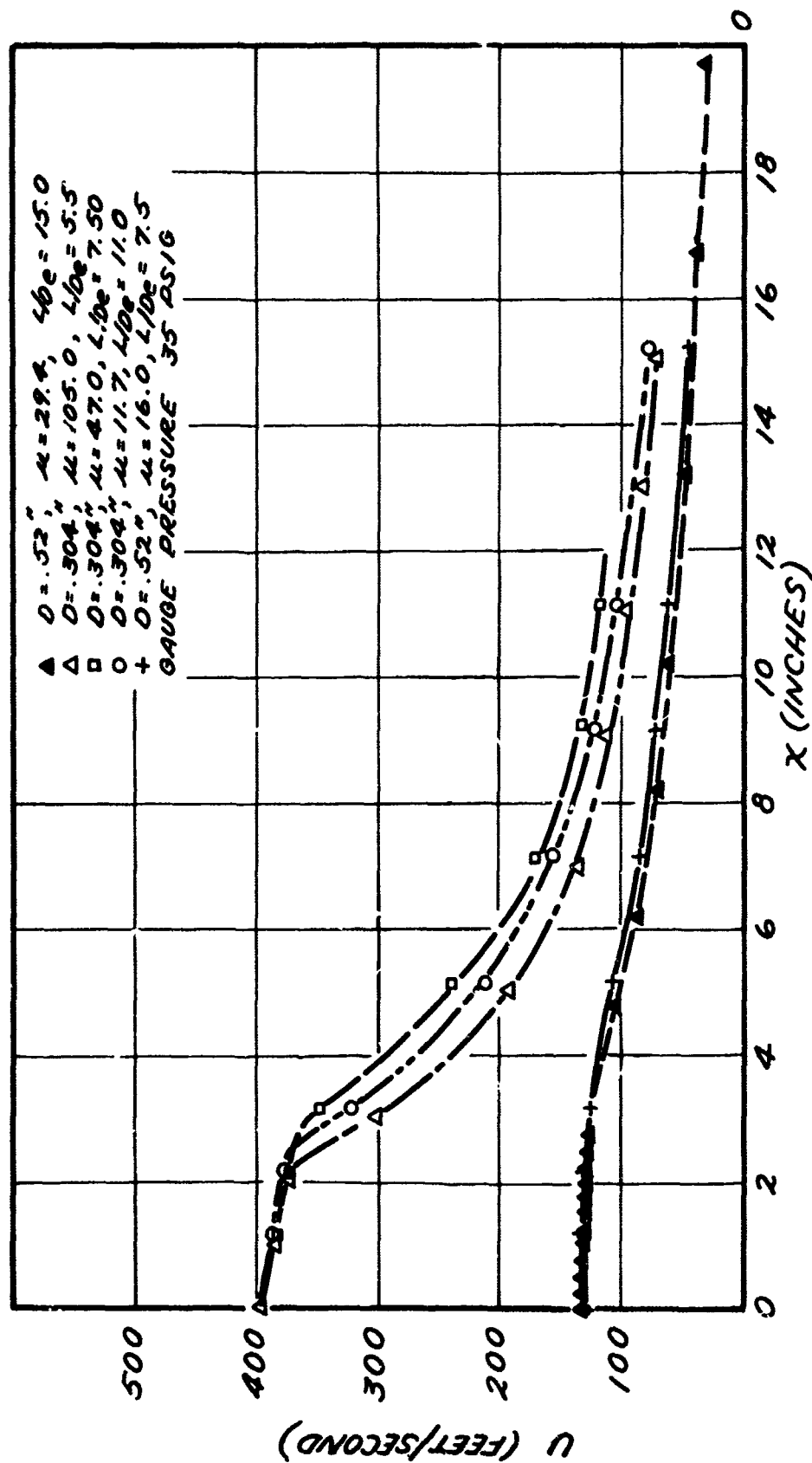Figure 23.   Velocity Profiles, μ = 105.5.

44

Figure showing velocity profiles. Legend:

X/D = 1.44 (×)
X/D = 3.36 (+)
X/D = 5.30 (⊙)
X/D = 9.14 (□)
X/D = 15.90 (△)
X/D = 19.70 (⊖)
X/D = 25.50 (⊕)
X/D = 32.20 (⊘)
X/D = 38.00 (●)
X/D = 68.80 (∅)

μ = 29.4
U/Ue = 15.0

Vertical axis: U/Ue, from 0.0 to 1.0
Horizontal axis: U/U, from 0.00 to 1.4

45

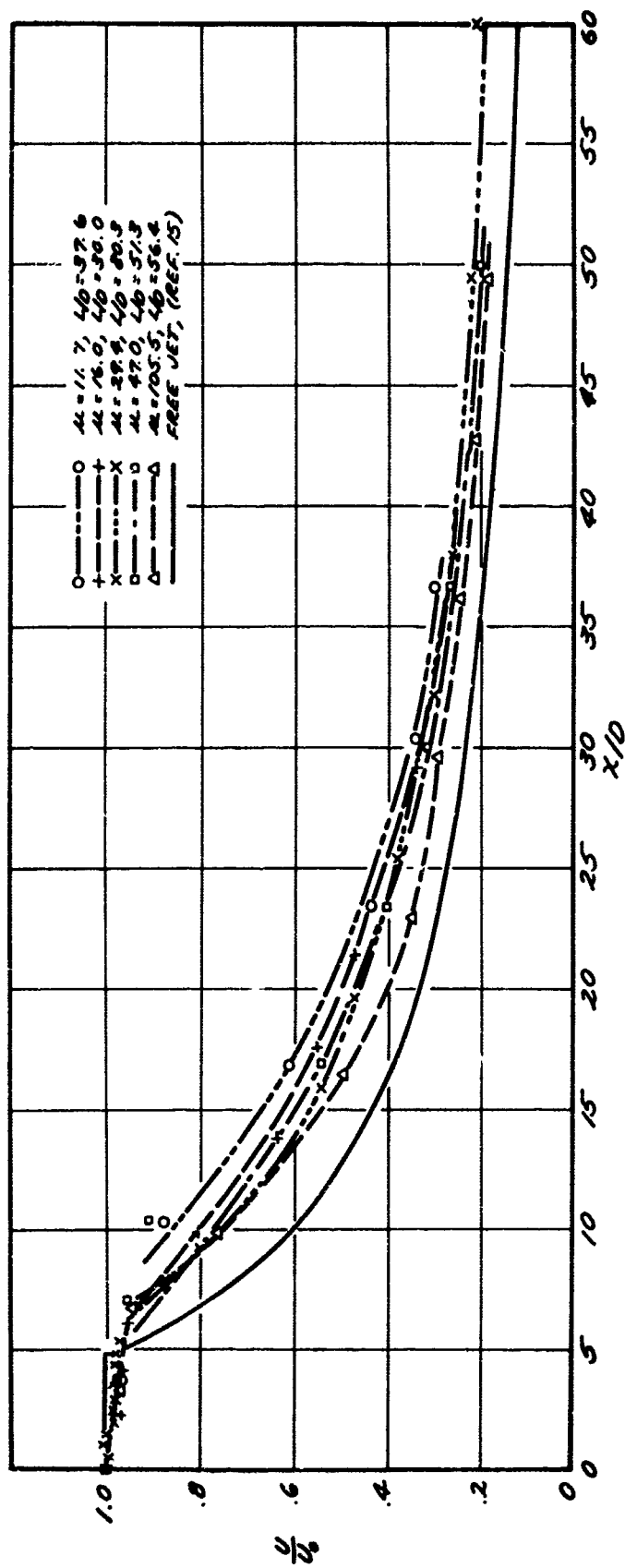Figure 25. Variations of Centerline Velocity Along the Length of Ejector.

Figure 26. Comparison of Theoretical and Experimental Centerline Velocity Ratio of Ejectors and That of a Free Jet.
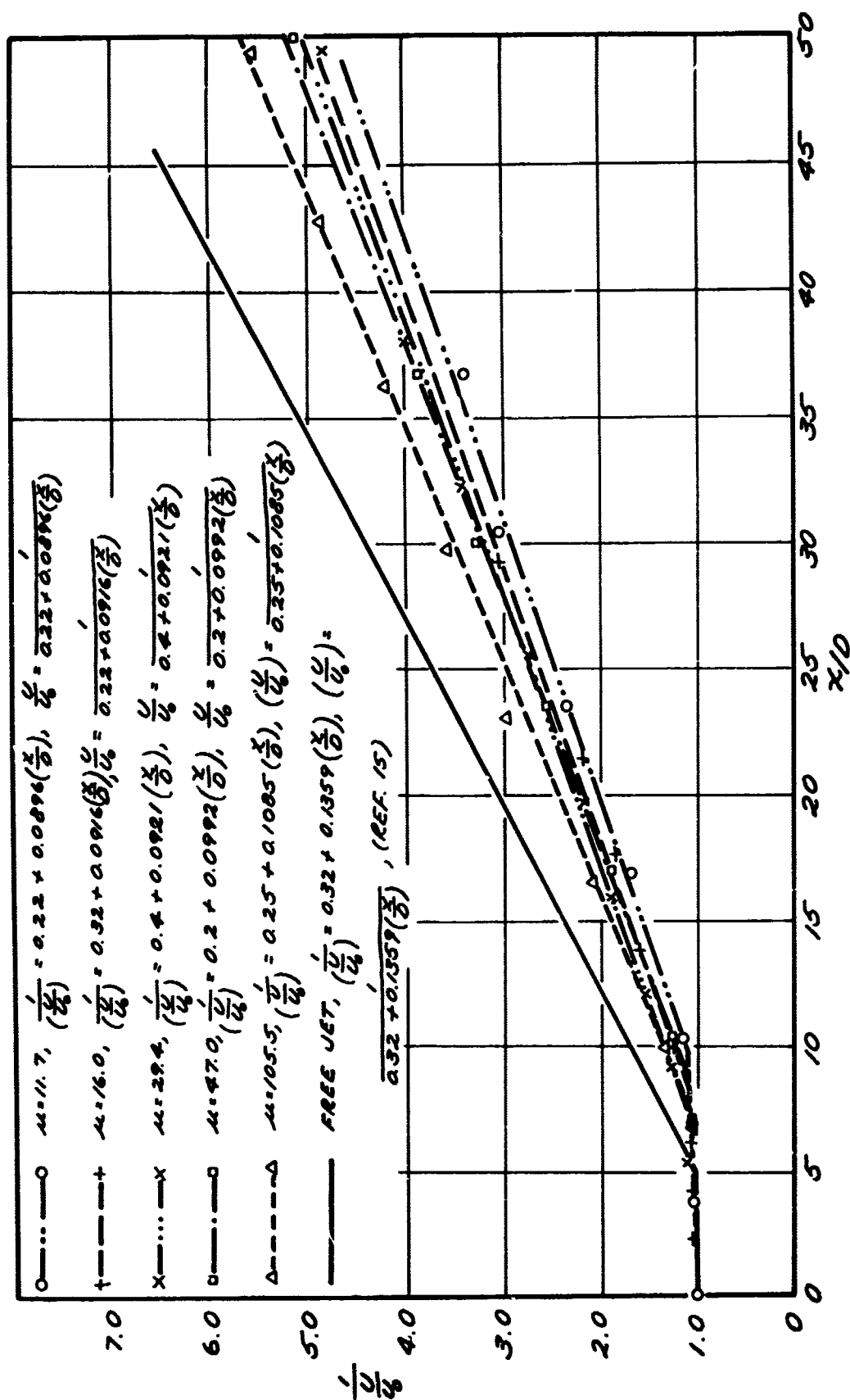
47

Figure 27. Comparison of Theoretical and Experimental Inverse Centerline Velocity
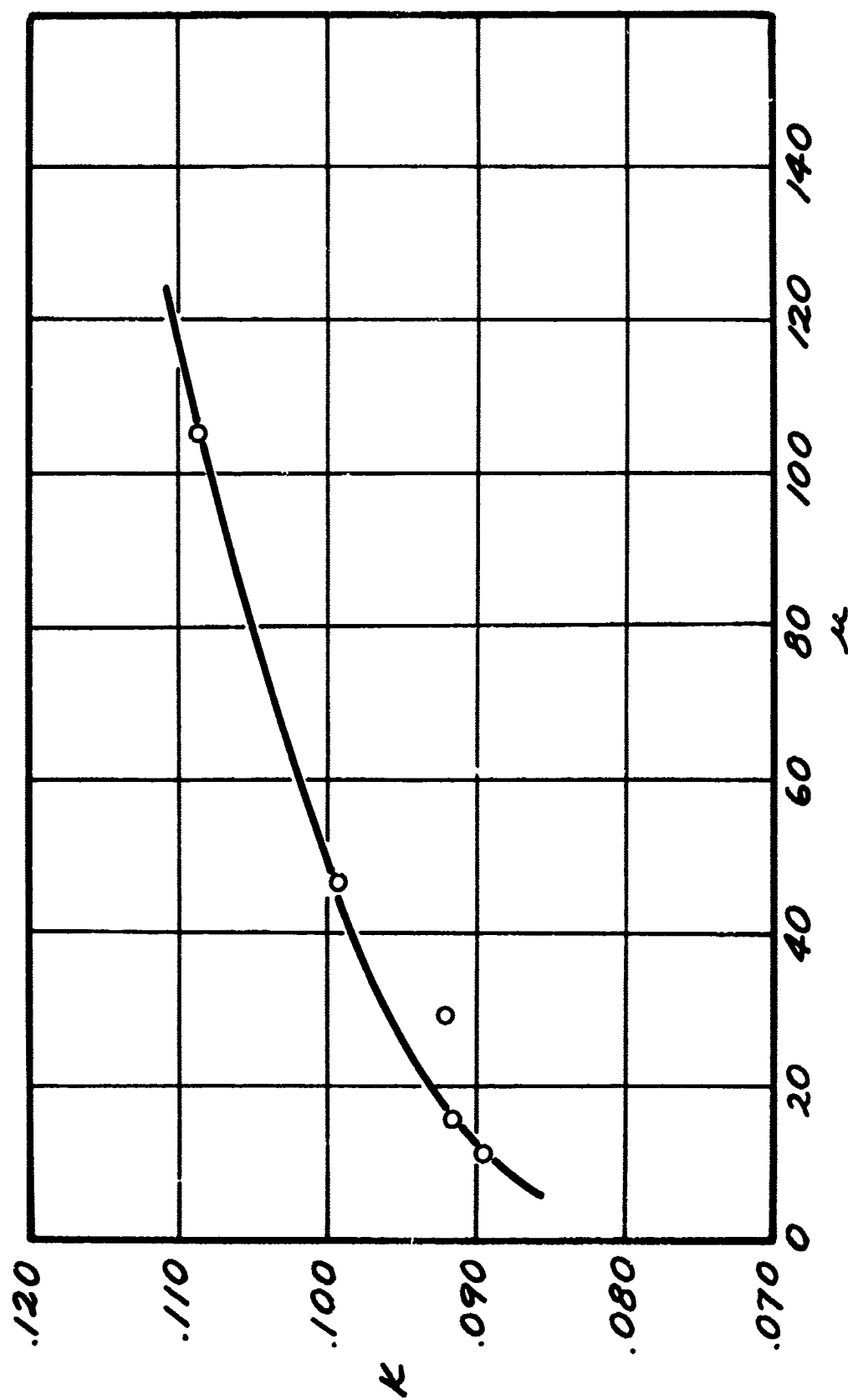Ratio of Ejectors and That of a Free Jet.

48

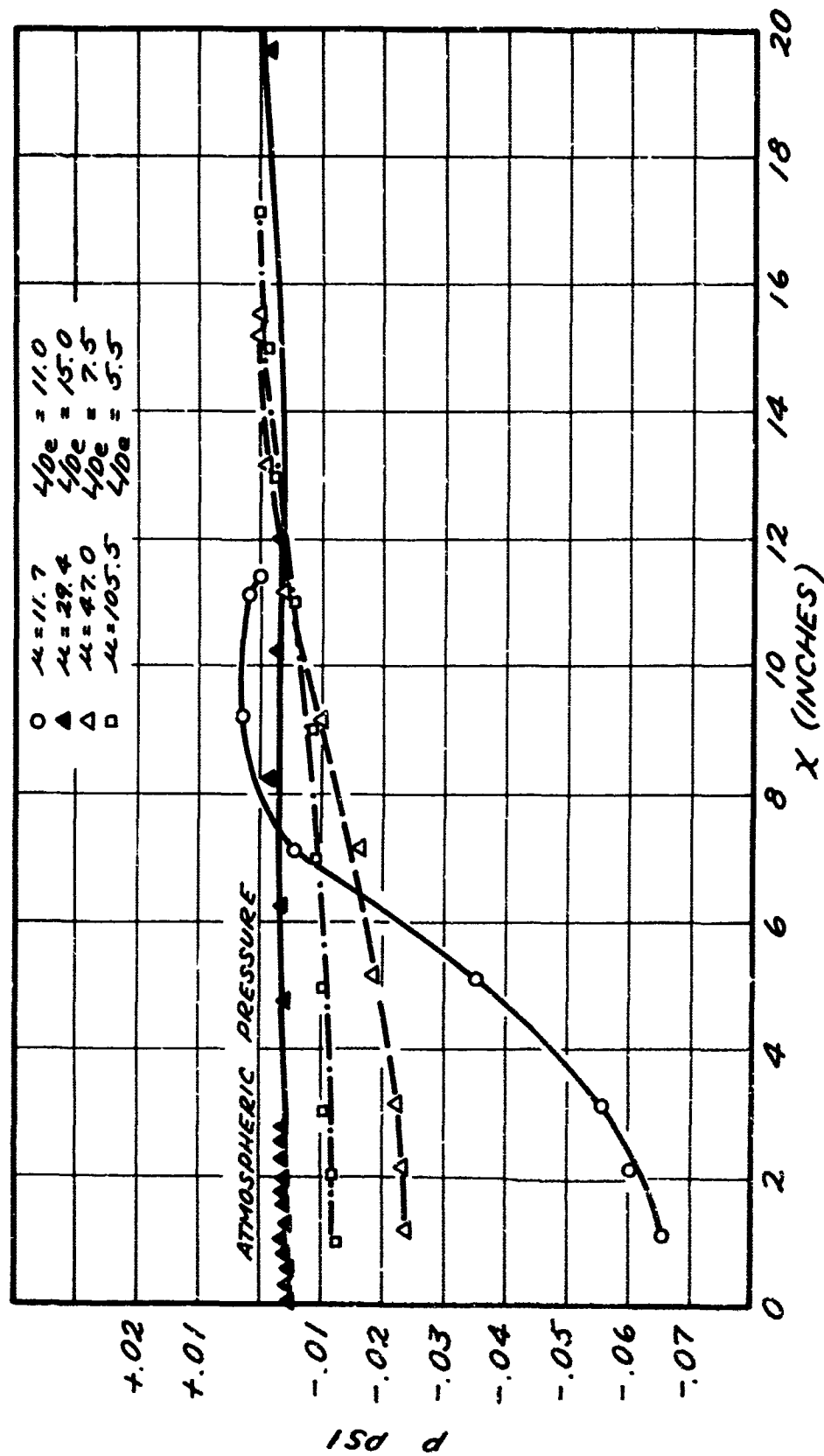Figure 28. Effect of Area Ratio on k.

Figure 29. Variations of Pressure Along the Length of Ejectors.

TABLE 1		
THE DIMENSIONS OF THE EXTENSIONS OF NOZZLES		
Nozzle No.	Inside Diameter of Exits (inches)	Extension Lengths (inches)
1	0.304	0.54, 1.15, 2.12, 4.13
2	0.520	0.60, 1.10, 2.10, 4.15

TABLE 2			
THE DIMENSIONS OF THE EJECTORS			
Ejector No.	Inside Diameter (inches)	No. of Short Ejectors	Length (inches)
1	1.04	5	11.40
2	2.08	6	15.60
3	3.12	6	17.15
4	2.82	-	42.00

TABLE 3

AXIAL LOCATIONS WHERE VELOCITY
DISTRIBUTIONS WERE MEASURED

Ejector No.	Axial Distance from Initial Plane in Inches
1	0.00, 1.14, 2.14, 3.14, 5.14, 7.14, 9.24, 11.14
2	0.00, 1.16, 2.16, 3.16, 5.16, 7.16, 9.16, 11.16, 13.16, 15.20
3	0.00, 1.00, 2.03, 3.01, 5.00, 9.02, 11.02, 13.00
4	At an interval of 0.25 inches for the first 12 stations, 0.50 inches for the next 28 stations, and 2.00 inches for the last 6 stations.